



**HAL**  
open science

## Thermodynamics for clay minerals: Calculation tools and application to the case of illite/smectite interstratified minerals

Philippe Blanc, F. Gherardi, P. Vieillard, Nicolas C.M. Marty, H el ene  
Gailhanou, St ephane Gaboreau, Bruno Letat, C. Geloni, E.C. Gaucher,  
Beno t Made

### ► To cite this version:

Philippe Blanc, F. Gherardi, P. Vieillard, Nicolas C.M. Marty, H el ene Gailhanou, et al.. Thermody-  
namics for clay minerals: Calculation tools and application to the case of illite/smectite interstratified  
minerals. Applied Geochemistry, 2021, 130, pp.104986. 10.1016/j.apgeochem.2021.104986 . hal-  
03746374

HAL Id: hal-03746374

<https://brgm.hal.science/hal-03746374>

Submitted on 24 May 2023

**HAL** is a multi-disciplinary open access archive for the deposit and dissemination of scientific research documents, whether they are published or not. The documents may come from teaching and research institutions in France or abroad, or from public or private research centers.

L'archive ouverte pluridisciplinaire **HAL**, est destin ee au d ep ot et  a la diffusion de documents scientifiques de niveau recherche, publi es ou non,  emanant des  tablissements d'enseignement et de recherche fran ais ou  trangers, des laboratoires publics ou priv es.



Distributed under a Creative Commons Attribution - NonCommercial 4.0 International License

1 **Thermodynamics for clay minerals: calculation tools and application to the case of**  
2 **illite/smectite interstratified minerals**

3  
4 *P. Blanc*<sup>1\*</sup>, *Gherardi F.*<sup>2</sup>, *Vieillard P.*<sup>3</sup>, *Marty N.C.M.*<sup>1</sup>, *Gailhanou H.*<sup>1</sup>, *Gaboreau S.*<sup>1</sup>, *Letat B.*<sup>1</sup>,  
5 *Geloni C.*<sup>4</sup>, *Gaucher E.C.*<sup>5</sup>, *Madé B.*<sup>6</sup>

6  
7 <sup>1</sup>BRGM, 3 Avenue Claude Guillemin, 45060 Orléans Cedex 2, France

8 <sup>2</sup>IGG – CNR, Via G. Moruzzi, 56124 Pisa, Italy

9 <sup>3</sup>CNRS-IC2MP-UMR-7285 Hydrasa, 5 av. Albert Turpain, 86073 Poitiers Cedex, France

10 <sup>4</sup>Geological Laboratories, ENI S.p.A., San Donato Milanese, Italy.

11 <sup>5</sup>TOTAL S.A., Avenue Larribau, 64018 Pau, France

12 <sup>6</sup>ANDRA, 92298 Châtenay-Malabry, France.

13 \* Corresponding author : p.blanc@brgm.fr

14  
15  
16  
17 **Abstract**

18 We present two computing tools, ClayTherm and ISTherm, devoted to the estimation of the  
19 thermodynamic properties of both anhydrous and hydrated clay minerals (ClayTherm), and  
20 of illite/smectite (I/S) mineral series (ISTherm). The first computing tool, ClayTherm, is  
21 devoted to thermodynamic property estimates for clay minerals. It combines several  
22 previously published estimation models, including hydration aspects. Verification is provided,  
23 against a set of solubility data, selected from previous literature. A specific application  
24 ISTherm was subsequently developed based on the first tool. It focuses on the smectite-to-  
25 illite transformation, and is able to calculate the thermodynamic properties of a series of  
26 illite/smectite (I/S) interstratified minerals, starting from the composition of a single I/S  
27 sample. The thermodynamic functions have been completed for the mixing energies and the  
28 tool was then used in order to investigate the case of a natural I/S hydrothermal series from  
29 the Shinzan geothermal field (Japan). Activity diagrams have been calculated including  
30 illite/smectite and phase relations are found to be in agreement with previous mineralogical  
31 observations and solution chemical analyses. The I/S series from Shinzan is further  
32 investigated through reactive transport modelling by using a site-specific, augmented version  
33 of the geochemical database. Illitization through the formation of I/S is predicted over realistic  
34 reaction times, consistently with available mineralogical observations.

35  
36  
37  
38 *Keywords:* Thermodynamics, clay minerals, interstratified illite/smectite, environment  
39  
40

42 Knowledge of the thermodynamic properties of clay minerals is essential for the prediction of  
43 the chemical behaviour of clayrock, soils or artificial materials (engineered barriers, additives,  
44 drugs, etc.) in various sub-surface geological systems (Velde, 1992). Such knowledge is  
45 needed to precisely model the chemical composition of clayrock porewaters (Gaucher et al.,  
46 2009) or the interactions between engineered clay barriers and concrete (Marty et al., 2009)  
47 in the context of deep disposal of radioactive waste. In the nuclear waste management  
48 context, clay minerals are considered as good candidates for waste confinement barriers due  
49 to their low permeability, high plasticity and adsorption properties (Landais, 2006). This is  
50 especially the case of materials containing large amounts of smectites. In order to assess the  
51 stability of barrier concepts over long periods of time (more than 100,000 years),  
52 geochemical modelling is a valuable tool for predicting mineralogical and chemical  
53 evolutions. Thermodynamic properties are essential for such applications but they are still  
54 poorly understood for clay minerals, with little unambiguous experimental data available. This  
55 work first presents the development of a computing tool, combining several previously  
56 published estimation models, including 7, 14 and 10Å phases, and, for the latter, offering the  
57 capacity to hydrate in contact with aqueous solution.

58  
59 Illite/smectite mixed layer clay minerals (I/S) are widely present in the natural environment  
60 and occur in various contexts, notably during diagenetic processes in sedimentary basins  
61 (Hower and Mowatt, 1966), or hydrothermal alteration of volcanic rocks (Inoue, 1983).  
62 Understanding the processes associated with the transformation of smectite into  
63 illite/smectite and its consequences on mechanical and geochemical behaviour for clay  
64 formation is of great importance in some major application fields, such as oil exploration  
65 (Geloni et al., 2017) or nuclear waste disposal (Meunier et al., 1998), CO<sub>2</sub> storage in  
66 underground reservoirs (Gherardi and Audigane, 2014; Wertz et al., 2013) or for geothermal  
67 field exploration (Battaglia et al., 2013). For instance, smectite-to-illite conversion reactions  
68 may generate overpressure in sedimentary basins due to the dehydration of smectite that  
69 can be problematic for oil well production (Tremosa et al., 2020). Based on the chemical  
70 analyses of natural I/S samples, Meunier and Velde (1989) described interstratified  
71 illite/smectite using a ternary composition model (one illite and two montmorillonite end-  
72 members). Based on this approach, Blanc et al. (1997) developed a solid solution model  
73 allowing the calculation of the energies of mixing of illite and smectite layers depending on  
74 the degree of order of the stacking sequences.

75  
76 This work brings the opportunity to develop a specific calculation tool able to determine the  
77 composition of these end-members based on the composition of a single I/S sample. The  
78 tool itself corresponds to an evolution of a previous development proposed by Geloni et al.  
79 (2017), implementing intermediate composition calculations. For the thermodynamic  
80 calculation, the tool systematizes the approach proposed previously by Gailhanou et al.  
81 (2019), including an assessment of the non-ideal mixing energies. The method is illustrated  
82 using a previously documented case of hydrothermal smectite illitization, i.e. the Shinzan  
83 area series (Inoue and Utada, 1983).

84

## 2. Previous advances and context

87 Until now, much of the available thermodynamic data for clay minerals have been derived  
88 either from solution experiments or from predictive calculations. Numerous experimental  
89 studies of equilibration in solution have been conducted since the pioneering work of  
90 Reesman and Keller (1968). Equilibration experiments on illite were repeated by Kittrick  
91 (1984) and Aja et al. (1991). The case of smectite was investigated, among others, by  
92 Reesman and Keller (1968), May et al. (1986), and Kittrick and Peryea (1988). Essene and  
93 Peacor (1995) criticised the solution experiments and the properties derived from these  
94 studies have not been included so far in the usual thermodynamic databases for  
95 geochemical modelling. To overcome such issues, calorimetric measurements have been  
96 carried out in the last decade, on a variety of clay minerals, following methods which are  
97 described in detail by Gailhanou et al. (2007, 2009, 2012 and 2013) and Blanc et al. (2014).  
98 A compilation of the measured thermodynamic properties is provided by Blanc et al. (2015).  
99 Recently, Gaboreau et al. (2020) showed, for four clay mineral samples, that solution  
100 experiments could provide thermodynamic properties close to calorimetric measurements.  
101 This result was achieved under the following conditions: (i) equilibration experiments lasting  
102 at least two (2) years, and (ii) reaction temperature increasing from 25 to 40°C, to enhance  
103 equilibration kinetics. Note that both calorimetry and solubility experiments were performed  
104 on the same samples.

105  
106 For decades, estimation methods (Chermak and Rimstidt, 1989; Van Hinsberg et al., 2005a,  
107 b; Vieillard, 2000, 2002) remained the usual source of thermodynamic data for clay minerals,  
108 although neither parametrization nor verification could be assessed against the  
109 thermodynamic properties of actual clay minerals. Blanc et al. (2015) proposed a model,  
110 based on Vieillard and Tardy (1988), Vieillard (1994a), Vieillard (1994b) and on Chermak and  
111 Rimstidt (1989) formalisms to estimate the whole set of thermodynamic properties ( $\Delta_f H^0$ ,  $S^0$ ,  
112  $C_p^0(T)$  and even  $V^0$ ). The model was parameterized and verified, on the basis of properties  
113 extracted from calorimetric measurements performed on actual clay minerals. Unfortunately,  
114 the model by Blanc et al. (2015) only applies to anhydrous phases, and it cannot be verified  
115 with respect to the experimental data and the compilation of solubility constants recently  
116 provided by Gaboreau et al. (2020).

117  
118 To overcome this difficulty, H<sub>2</sub>O vapour isotherms were measured by Gailhanou et al. (2017)  
119 and Vieillard et al. (2019), and the results were gathered to develop a hydration model able  
120 to predict thermodynamic properties of hydration over a large range of clay mineral  
121 compositions. Combining the approaches developed by Blanc et al. (2015), Gailhanou et al.  
122 (2017) and Vieillard et al. (2019) would allow the prediction capacities to be tested with  
123 respect to solubility data obtained or selected by Gaboreau et al. (2020). A similar approach  
124 was proposed by Vidal and Dubacq (2009) and Dubacq et al. (2010). In our case,  
125 parameterization and verification are performed based on thermodynamic properties  
126 measured specifically on clay minerals. The model developed by Vidal and Dubacq (2009)  
127 and Dubacq et al. (2010) is based on Chermak and Rimstidt (1989) work, for the anhydrous  
128 part. This latter work had been improved in a version specifically devoted to clay minerals by  
129 Blanc et al. (2015), providing estimates more accurate for this specific group of minerals.

130  
131 The approaches developed by Blanc et al. (2015), Gailhanou et al. (2017) and Vieillard et al.  
132 (2019) can be combined according to the workflow displayed in Figure 1. Ultimately, it allows  
133 equilibrium constants to be predicted for clay minerals and a comparison of the calculated  
134 thermodynamic properties to be made with respect to solubility data selected from the  
135 literature.

137  
138

### 3. Theoretical background

139  
140  
141  
142  
143  
144  
145  
146

Classic thermodynamic relations and conventions theoretically apply to clay minerals as with any other mineral. Consequently, the formation properties of a clay mineral will depend on the definition of a reference state. The reference state is considered as the standard state, at 1 bar and 298.15K. Following Helgeson et al. (1978), the pressure between the temperature interval 273.15 to 373.15K is constant, at 1 bar. For  $T > 373.15\text{K}$  ( $100^\circ\text{C}$ ), the pressure is obtained from the water liquid-vapour curve. Considering a phase AB, its apparent Gibbs free energy of formation  $\Delta_a G_{AB,P,T}^0$  is given, at P and T, by the relation:

$$\begin{aligned} \Delta_a G_{AB,P,T}^0 &= \Delta_f H_{AB,P,T}^0 - T \cdot S_{AB,P,T}^0 \\ &= \Delta_f H_{AB,P_r,T_r}^0 - T \cdot S_{AB,P_r,T_r}^0 + \int_{T_r}^T C_{p,AB}^0 dT - T \cdot \int_{T_r}^T \frac{C_{p,AB}^0}{T} dT + \int_{P_r}^P V_{AB}^0 dP \end{aligned} \quad (1)$$

149  
150  
151  
152  
153  
154

where  $T_r$ : temperature at the reference state (298.15 K);  $P_r$ : pressure at the reference state (0.1 MPa);  $\Delta_f H_{AB,P,T}^0$ : enthalpy of formation of the phase AB at temperature T and pressure P;  $S_{AB,P,T}^0$ : the third law entropy of the AB phase;  $C_{p,AB}^0$ : heat capacity of the AB phase;  $V_{AB}^0$ : molar volume of the AB phase, independently of temperature.

This definition follows the Benson–Helgeson convention (Benson, 1968; Helgeson et al., 1978) where  $\Delta_a G_{AB,P,T}^0$  equals  $\Delta_f G_{AB,P,T}^0$  only at  $25^\circ\text{C}$ . The heat capacity function is related to the dependence of entropy and formation enthalpy with temperature through:

$$\Delta_a H_{AB,P,T}^0 = \Delta_f H_{AB,T_r}^0 + \int_{T_r}^T C_{p,AB}^0 dT \text{ and } S_{AB,P,T}^0 = S_{AB,T_r}^0 + \int_{T_r}^T \frac{C_{p,AB}^0}{T} dT \quad (1)$$

The third law entropy term, at  $T_r$ , includes the heat capacity function, and a residual contribution:

$$S_{AB,P_r,T_r}^0 = \int_0^{T_r} \frac{C_{p,AB}^0}{T} dT + S_{AB}^{\text{mag}} + S_{AB}^{\text{conf}} \text{ where } \int_0^{T_r} \frac{C_{p,AB}^0}{T} dT = S_{AB,P_r,T_r}^{\text{lat}} \quad (3)$$

with  $S_{AB,P_r,T_r}^{\text{lat}}$  standing for the lattice entropy. The two first terms in Equation (3) can be measured by low temperature calorimetry (PPMS or adiabatic, Gailhanou et al. (2012)) and  $S_{AB}^{\text{mag}}$  represents the magnetic entropy (Holland, 1989). For the configuration entropy term  $S_{AB}^{\text{conf}}$ , Ulbrich and Waldbaum (1976) proposed a calculation method for assessing the maximum value of both the magnetic and the configurational entropy terms. For the  $S_{AB}^{\text{conf}}$  term, the method is based on a site mixing approach and for the magnetic contribution, on the maximum number of spin configurations according to:

$$S_{AB}^{\text{mag}} = R \sum_i x_i^{\text{AB}} \ln(2S_i + 1) \quad (4)$$

where R is the gas constant,  $x_i^{\text{AB}}$  the mole fraction of element i in solid AB, and  $S_i$  its spin number. This expression is valid for the metals of the first transition series for which the valence electrons are in the outermost shells.

177

178 The illite/smectite case needs to define solid solution properties. Considering a second solid  
 179 phase CB, its Gibbs free energy  $\Delta_f G_{SS,P,T}^0$  results from the combination of both end-members'  
 180 Gibbs free energy,  $\Delta_f G_{AB,P,T}^0$  and  $\Delta_f G_{CB,P,T}^0$  by :

$$181 \Delta_f G_{SS,P,T}^0 = x \cdot \Delta_f G_{AB,P,T}^0 + (1 - x) \Delta_f G_{CB,P,T}^0 + \Delta G_{SS,P,T}^{mix} \quad (5)$$

182 where  $x$  and  $\Delta G_{SS,P,T}^{mix}$  correspond respectively to the fraction of AB end-member and the  
 183 Gibbs energy of mixing. The latter can be decomposed into enthalpy  $\Delta H_{SS,P,T}^{mix}$  and entropy  
 184  $\Delta S_{SS,P,T}^{mix}$  of mixing terms:

$$185 \Delta G_{SS,P,T}^{mix} = \Delta H_{SS,P,T}^{mix} - T \cdot \Delta S_{SS,P,T}^{mix} \quad (6)$$

186 The entropy of mixing can be estimated, to a first approximation, considering an ideal mixing  
 187 between end-members, resulting in:

$$188 \Delta S_{SS,P,T}^{mix} = -R \cdot [x \ln(x) + (1 - x) \ln(1 - x)] \quad (7)$$

189 As for the equilibrium of AB in an aqueous solution, we consider the dissolved species  $A^+$   
 190 and  $B^-$  and the chemical reaction:



192 Any reaction property  $\Delta_r \Xi_{AB,P,T}^0$  can be obtained from the corresponding formation property  
 193  $\Delta_f \Xi_{AB,P,T}^0$ , according to the relation:

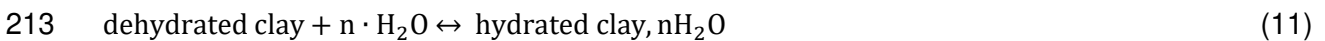
$$194 \Delta_r \Xi_{AB,P,T}^0 = \Delta_f \Xi_{A^+,P,T}^0 + \Delta_f \Xi_{B^-,P,T}^0 - \Delta_f \Xi_{AB,P,T}^0 \quad (9)$$

195 where  $\Xi$  stands for G, H or S, or any other property. Finally, the Gibbs free energy of reaction  
 196 (3) is related to the equilibrium constant of the reaction,  $K_{AB,P,T}$ , by:

$$200 \Delta_r G_{AB,P,T}^0 = -R \cdot T \cdot \text{Log} K_{AB,P,T} \cdot \ln(10) \quad (10)$$

$$201 \Delta_r G_{AB,P,T}^0 = -R \cdot T \cdot \log_{10} K_{AB,P,T} \cdot \ln(10)$$

202 Clay minerals may undergo hydration reactions (smectites and vermiculites). In more detail  
 203 (Gailhanou et al., 2017), a hydration reaction may be expressed by:



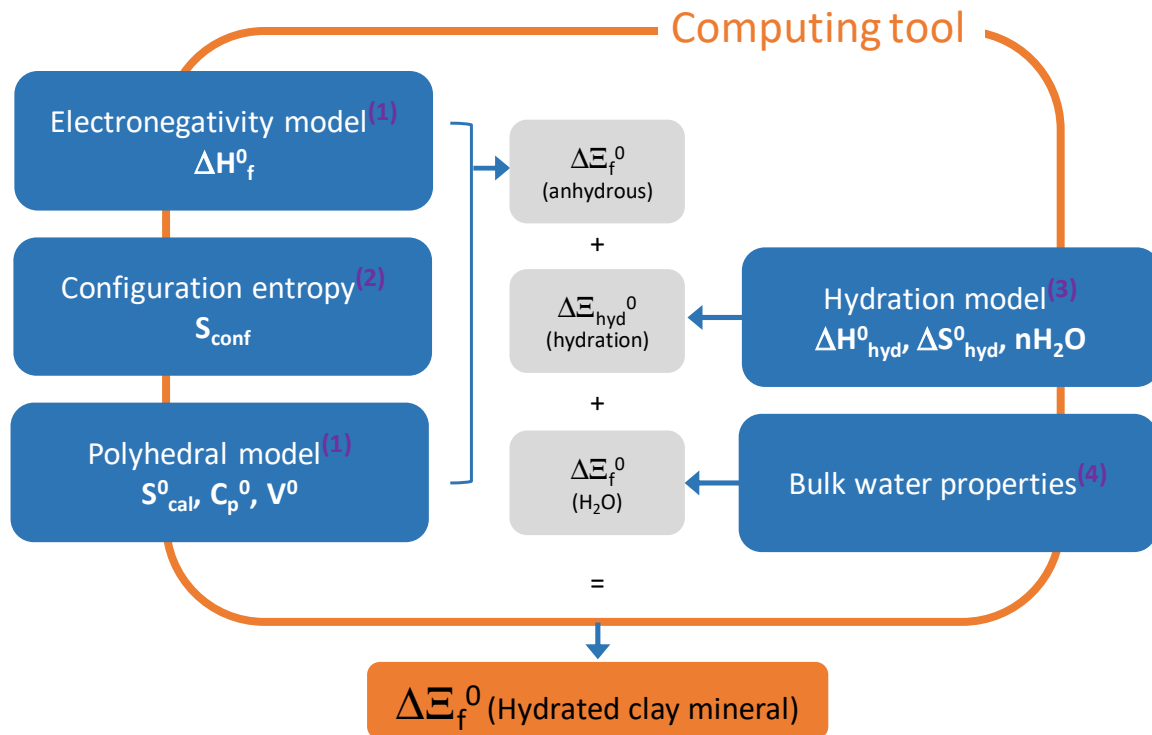
205 We can consider the property of hydration  $\Delta \Xi_{hyd,Tr}^0$  (per  $H_2O$  mole) for a given clay mineral  
 206 having  $n$  bounded molecules per half-cell. It is related to the total formation property  $\Delta \Xi_{f,Tr}^0$  of  
 207 the mineral through the following relation:

$$208 \Delta_f \Xi_{Pr,Tr}^0(\text{hydrated clay}) = \Delta_f \Xi_{Pr,Tr}^0(\text{anhydrous clay}) + n_{H_2O} \cdot \Delta_f \Xi_{Pr,Tr}^0(H_2O) + n_{H_2O} \cdot \Delta_{hyd} \Xi_{Pr,Tr}^0 \quad (12)$$

209 where  $\Delta_f \Xi_{Pr,Tr}^0(\text{hydrated clay})$ ,  $\Delta_f \Xi_{Pr,Tr}^0(\text{dehydrated clay})$  and  $\Delta_f \Xi_{Pr,Tr}^0(H_2O)$  stand for the  
 210 formation property for the hydrated mineral, the dehydrated mineral and the bulk water,  
 211 respectively.

212 Regarding clay minerals, in order to estimate the whole set of thermodynamic parameters,  
 213 including the hydration properties, it is necessary to combine models able to predict

228 anhydrous phase properties and models able to calculate the hydration properties. Such a  
 229 methodology had been previously followed by Vidal et al. (2009) and Dubacq et al. (2010),  
 230 who combined their own hydration model with Chermak and Rimstidt's work (1989), for the  
 231 anhydrous part. Similarly, in this study the estimation of thermodynamic properties for  
 232 hydrated clay minerals is achieved by merging the model of Blanc et al. (2015) for the  
 233 anhydrous part and the model developed by Gailhanou et al. (2017) and Vieillard et al.  
 234 (2019) for hydration. The whole process is illustrated in Figure 1.  
 235  
 236



<sup>(1)</sup> Vieillard et al. (1994a and b), Blanc et al. (2015) ; <sup>(2)</sup> Ulrich and Waldbaum (1976) ; <sup>(3)</sup> Gailhanou et al. (2017), Vieillard et al. (2019) ; <sup>(4)</sup> Cox et al. (1989)

237  
 238  
 239  
 240  
 241  
 242  
 243  
 244

Figure 1 – General scheme indicating the relations between estimation models to provide thermodynamic properties for hydrated clay minerals

245  
246

## 4. Generic estimation tool: ClayTherm

247 The calculation of cation sharing in crystallographic sites has been automated in a computing  
248 tool, giving the opportunity to improve the Blanc et al. (2015) model in terms of consistency  
249 and to provide additional verification cases. These aspects are described below.  
250

### 251 4.1. AUTOMATION OF CATION SHARING IN CRYSTALLOGRAPHIC SITES

252  
253 Minerals with d-spacings of 7, 10 and 14 Å contain M1 and M2 octahedral sites (1 M1 and 2  
254 M2 per  $O_{10}(OH)_2$ ). In Blanc et al. (2015), the sharing of cations was calculated based on a  
255 random distribution, with 2/3 of the cations entering M2 sites and 1/3 M1 sites. Such an  
256 assumption is valid for trioctahedral minerals, for which all sites are filled with mostly divalent  
257 species. For dioctahedral minerals with an octahedral composition dominated by trivalent  
258 species and composition close to 2 cations per  $O_{10}(OH)_2$ , automatically applying this sharing  
259 method implies creating vacancies in M2 sites, which does not correspond to current  
260 crystallographic observations (Brown, 1982). In this regard, the calculation should include a  
261 rule so as for dioctahedral minerals to fill in the M2 sites up until 2 cations per  $O_{10}(OH)_2$ .  
262 Additional cations, for a dioctahedral mineral with more than 2 octahedral cations, are  
263 thereafter entering the M1 site. The limit to this infilling process was pointed out by Yamada  
264 et al. (1999). They investigated the dioctahedral-trioctahedral 2:1 smectite join, from  
265 experiments and reviewing previous literature data. They concluded that there was a large  
266 miscibility gap between 2.33 and 2.66 cations per  $O_{10}(OH)_2$ . Following this, starting from 2 up  
267 to 2.33 cations per  $O_{10}(OH)_2$ , M1 and M2 sites are filled proportionally to the relative  
268 amounts. From 2.33 to 2.66 cations, no phase should be stable and between 2.66 and 3  
269 cations, the mineral is reported to be trioctahedral, without cation preferences between M1  
270 and M2 sites (Yamada et al., 1999). Eastonite  $K(Mg_2Al)(Si_2Al_2)O_{10}(OH)_2$ , an end-member of  
271 the biotite solid solution, represents a specific case. Circone and Navrotsky (1992) reported,  
272 based on infrared and Raman spectra of Mg-Al-biotite, that Al orders onto the M1 site. Al  
273 ordering in M1 is considered in the model developed by Blanc et al. (2015). This type of  
274 ordering is implemented as a specific option, which also applies to siderophyllite. The  
275 option also includes Si, Al ordering between T1 and T2 tetrahedral sites. Globally, the  
276 thermodynamic properties of biotite solid solution end-members phlogopite, annite, eastonite  
277 and siderophyllite can be correctly estimated. But for intermediate compositions, neither  
278 miscibility gaps nor the cation order/disorder relations (Dachs and Benisek, 2019) have been  
279 implemented, so far. This limits the use of the tool for minerals belonging to the Biotite group.  
280

281 Regarding (Si, Al) sharing in T1 and T2 tetrahedral phyllosilicate sites, Vinograd (1995)  
282 compiled the measurements performed on many silicates (including phyllosilicates). He  
283 concluded that (Si, Al) ordering was only partial among the tetrahedral sites, according to the  
284 Homogeneous Distribution of Charge (HDC) hypothesis and depending on the  $Al/(Al+Si)$   
285 ratio. Globally, for an  $Al/(Al+Si)$  ratio from 0 to 0.1, few analyses are available in the literature  
286 and the distribution model impact on entropy is limited. For an  $Al/(Al+Si)$  ratio above 0.35, the  
287 Al-ordering between T1 and T2, corresponding to the Al-avoidance rule, would apply. At an  
288  $Al/(Al + Si)$  ratio ranging from 0.2 to 0.35, a distribution based on the HDC hypothesis would  
289 provide better consistency with Vinograd (1995). The three distributions, i.e. disordered,  
290 ordered and HDC (Vinograd, 1995), are implemented in the present calculation tool.  
291

292 For 10Å minerals, the entropy contribution of the interlayer configuration sites is calculated  
293 according to the Ulbrich and Waldbaum (1976) method, including mixing with vacancies. For  
294 the 14Å mineral brucite layer, sharing is calculated according to the Holland and Powell

295 (1998) method. The latter consists in distributing Al preferentially in the M4 site, then  
296 randomly sharing the remaining octahedral cations in the M1, M2 and M3 sites.  
297

298 For most of the 7Å minerals, the chemical composition does not greatly differ from that of the  
299 end-members. In this case, there is a general tendency to neglect the configurational entropy  
300 contribution (Bertoldi et al., 2005; Blanc et al., 2014), which we adopted here. Similarly and  
301 following Hemingway et al. (1984), the configurational contribution was not considered in this  
302 work for 14Å minerals. In contrast and following Holland (1989), for 10Å minerals Blanc et al.  
303 (2015) considered both the configuration and the additional terms of the magnetic entropy,  
304 whose calculation is also included in the overall calculation, consistently to Equation (3).  
305

## 306 4.2. EXTENDING THE COMPOSITION LIMITS OF PREVIOUS MODELS

307  
308 In the work presented by Blanc et al. (2015), the chemical elements which can be considered  
309 for both entropy and enthalpy estimates do not exactly match. The development reported in  
310 this article provides an opportunity to improve consistency, from this point of view. For  $S^{\text{lat}}$ ,  
311  $C_p^0$  and  $V^0$  estimates, the basic unit properties have been assessed according to the method  
312 described by Blanc et al. (2015), for interlayer  $\text{NH}_4^+$ , octahedral  $\text{Cd}^{2+}$  and tetrahedral  $\text{Fe}^{3+}$   
313 (see Table 1). It allows the set of basic units to be completed, consistently with the elements  
314 considered for enthalpy estimates by Blanc et al. (2015).  
315  
316

317 *Table 1 - Thermodynamic properties for additional polyhedral units (after Blanc et al. 2015)*

	$S^{\text{lat}}$	$C_p^0$	$V^0$
	J.mol <sup>-1</sup> .K <sup>-1</sup>	J.mol <sup>-1</sup> .K <sup>-1</sup>	cm <sup>3</sup> .mol <sup>-1</sup>
[int](NH <sub>4</sub> ) <sub>2</sub> O	364.50	247.63	38.16
[6]CdO	52.23	41.95	13.11
[4]Fe <sub>2</sub> O <sub>3</sub>	66.62	101.33	27.29

318 Bracketed numbers: correspond to the coordination of the cation in the  
319 phyllosilicate structure  
320

## 321 4.3. IMPLEMENTATION OF THE CALCULATION IN CLAYTHERM

322  
323 The tool ClayTherm was developed in Visual Basic©, under the Excel© interface. It  
324 estimates the formation and reaction properties for 7, 10 and 14Å anhydrous minerals and  
325 10Å hydrated phases. To facilitate the implementation in most geochemical databases, the  
326 temperature dependence of the equilibrium constant,  $\log_{10}K(T)$ , is calculated for 8  
327 temperatures (0, 25, 60, 100, 150, 200, 250, 300°C), using the  $C_p$  constant approximation,  
328 and the parameters A, C and D for the function  $\log_{10}K(T) = A + C/T + D \cdot \log_{10}(T)$  are  
329 provided. Thermodynamic properties of ions are issued from the Thermochimie database  
330 (Giffaut et al., 2014) and are consistent with the Thermodem database (Blanc et al., 2012).  
331 The sharing of the cations throughout the different crystallographic sites is calculated  
332 automatically, according to the rules previously reported.  
333

## 334 4.4. TESTING OF CLAYTHERM

335  
336 A first testing phase was conducted by running the tool for phases considered by Blanc et al.  
337 (2015) and Vieillard et al. (2019). A second testing phase was conducted by comparing the  
338 solubilities obtained by Gaboreau et al. (2020) with predicted values. The work on  
339 illite/smectite provides an opportunity for additional testing (see below).

#### 341 **4.4.1. Comparison with Blanc et al. (2015) and Vieillard et al. (2019) datasets**

342 The minerals used to parameterize the model developed by Blanc et al. (2015) (Table 12,  
343 Blanc et al. 2015) were first tested, to check the consistency of the tool developed here:

- 344 - 14Å minerals: (Si, Al) ordered, no deviation
- 345 - 10Å minerals: HDC Vinograd (1995) model except for eastonite and siderophyllite (Si,  
346 Al), the ordered octahedral layer and for paragonite which is (Si, Al) ordered. A  
347 typographical error was detected in Blanc et al. (2015) where paragonite  $S^{\text{lat}}$  should  
348 equal 305.20 instead of 305.31  $\text{J}\cdot\text{mol}^{-1}\cdot\text{K}^{-1}$
- 349 - 7Å minerals: (Si, Al) ordered, no deviation.

350

351 For the 10Å anhydrous and hydrated end-members calculated in Blanc et al. (2015) (Table  
352 14) and Vieillard et al. (2019) (Table 8), the results are identical using the HDC ordering  
353 model. Two differences arises for the 7Å minerals Berthierine(Fell) and Cronstedtite (Blanc  
354 et al. 2015, Table 14). Berthierine(Fell)  $\Delta_f H^0$  displays a typographical error in Blanc et al.  
355 (2015) with

356 -3770.46 instead of -3775.46  $\text{kJ}\cdot\text{mol}^{-1}$ , the correct value provided by ClayTherm. For  
357 Cronstedtite, the calculation from Blanc et al. (2015) was limited by using a  $^{44}\text{Fe}_2\text{O}_3$   
358 component assessed using Goethite properties. Now this component is fully integrated in  
359 ClayTherm which modifies the thermodynamic properties:

- 360 - Blanc et al. (2015):  $\Delta_f H^0 = -2914.55 \text{ kJ}\cdot\text{mol}^{-1}$ ;  $S^{\text{lat}} = 256.60 \text{ J}\cdot\text{mol}^{-1}\cdot\text{K}^{-1}$ ;  $C_p^0 = 257.02$   
361  $\text{J}\cdot\text{mol}^{-1}\cdot\text{K}^{-1}$ ;  $V^0 = 76.80 \text{ cm}^3\cdot\text{mol}^{-1}$
- 362 - This work:  $\Delta_f H^0 = -2916.68 \text{ kJ}\cdot\text{mol}^{-1}$ ;  $S^{\text{lat}} = 289.91 \text{ J}\cdot\text{mol}^{-1}\cdot\text{K}^{-1}$ ;  $C_p^0 = 307.69 \text{ J}\cdot\text{mol}^{-1}\cdot\text{K}^{-1}$ ;  
363  $V^0 = 90.44 \text{ cm}^3\cdot\text{mol}^{-1}$

364

365 On the whole, the comparison with the results of Blanc et al. (2015) and Vieillard et al. (2019)  
366 confirms that ClayTherm results are correct for most clay minerals. It allows typographical  
367 errors to be corrected and the predicted properties of cronstedtite to be improved, with  
368 respect to Blanc et al. (2015).

369

#### 370 **4.4.2. Comparison with solubility datasets**

371

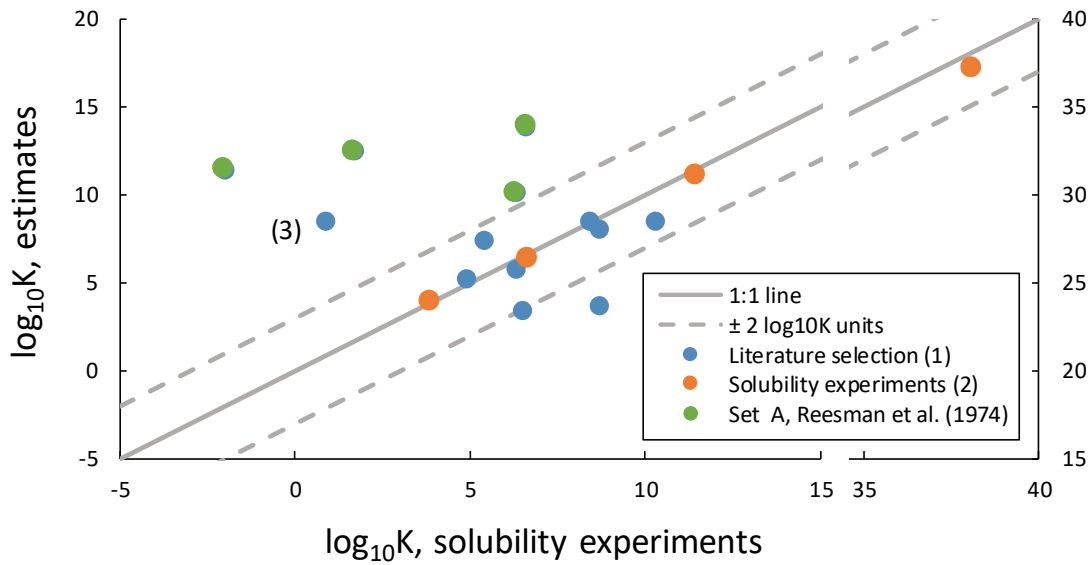
372 Vieillard et al. (2019) proposed a first selection of solubility data from the literature and  
373 comparison with  $\log_{10}K$  (298.15 K) estimates gives an average of  $\pm 2.5 \log_{10}$  units. The  
374 selection was recently refined by Gaboreau et al. (2020) who also reported a new set of  
375 experimentally measured solubilities for clay minerals: kaolinite, smectite, illite, vermiculite  
376 and chlorite. For the latter, equilibrium was clearly not reached, even after 2 years of  
377 equilibration at 40°C. Additionally, they selected a set of solubility experiments, from previous  
378 literature. Both sets were used in the present study to assess the estimates obtained using  
379 ClayTherm.

380

381 Results for the testing of the set of solubility data obtained by Gaboreau et al. (2020) are  
382 reported in Table 2. Globally, estimates correspond to solubilities with a rather low standard  
383 deviation between both values ( $\pm 0.41 \log_{10}$  units). Overall, the difference with estimates is  
384 larger when considering calorimetric data, especially due to the contribution of vermiculite  
385 (3.85  $\log_{10}$  units). The vermiculite Santa Ollala sample purified by Gailhanou et al. (2013) for  
386 the calorimetric measurements still contains an amount of impurities, like organic carbon, of  
387 which 0.42 wt. % still remains, even after  $\text{H}_2\text{O}_2$  treatment. Such impurity, not considered in  
388 the thermodynamic cycle used to derive formation enthalpy, could affect the correctness of  
389 the extracted value.

390

391 Standard deviations can be calculated from Table 2, for differences reported in columns 9  
 392 and 10. Without considering chlorite solubility, the standard deviation is  $\pm 1.3$  or  $\pm 0.4 \log_{10}$   
 393 units, depending whether or not calorimetry for vermiculite is considered. The average of  
 394 both standard deviations, i.e.  $\pm 0.9 \log_{10}$  units, produces a rather high uncertainty for  $\log_{10}K$   
 395 (298.15 K) estimates ( $\pm 1.7 \log_{10}$  units). This is still the most reasonable statement that can  
 396 be made concerning uncertainties for  $\log_{10}K$  (298.15 K) estimates in this work.  
 397  
 398



399  
 400 *Figure 2 – Comparison between log<sub>10</sub>K (298.15 K) ClayTherm estimates and results from*  
 401 *previous literature studies: (1) kaolinite, smectite, illite and vermiculite from Gaboreau et al.*  
 402 *(2020); (2) Illites and smectites from Gaboreau et al. (2020) literature selection.*  
 403  
 404  
 405  
 406

407

408 *Table 2 - Comparison between Gaboreau et al. (2020) experiment log<sub>10</sub>K (298.15 K) and ClayTherm estimates*

		Temp. (°C)	Solution exp. log <sub>10</sub> K <sup>(5)</sup>	(±)	Calorimetry log <sub>10</sub> K	(±)	Estimate log <sub>10</sub> K	Δ (Sol-Est) <sup>a</sup>	Δ (Cal-Est) <sup>b</sup>
Kaolinite KGa-2 <sup>(1)</sup>	Si <sub>2</sub> Al <sub>1.98</sub> Fe <sub>0.02</sub> O <sub>5</sub> (OH) <sub>4</sub>	40	6.61	0.70	6.46	0.60	6.40	0.21	0.06
Illite IMt-2 <sup>(2)</sup>	K <sub>0.762</sub> Na <sub>0.044</sub> (Si <sub>3.387</sub> Al <sub>0.613</sub> )(Al <sub>1.427</sub> Mg <sub>0.241</sub> Fe <sup>3+</sup> <sub>0.292</sub> Fe <sup>2+</sup> <sub>0.084</sub> ) O <sub>10</sub> (OH) <sub>2</sub>	25	11.42	0.70	11.52	1.60	11.15	0.27	0.37
Smectite MX80 <sup>(2)</sup>	Na <sub>0.409</sub> K <sub>0.024</sub> Ca <sub>0.009</sub> (Si <sub>3.738</sub> Al <sub>0.262</sub> )(Al <sub>1.598</sub> Mg <sub>0.214</sub> Fe <sup>3+</sup> <sub>0.173</sub> Fe <sup>2+</sup> <sub>0.035</sub> ) O <sub>10</sub> (OH) <sub>2</sub> ·5.189H <sub>2</sub> O	40	3.83	1.70	3.33	1.70	3.88	-0.05	-0.55
Vermiculite SO <sup>(3)</sup>	Ca <sub>0.445</sub> (Si <sub>2.778</sub> Al <sub>1.222</sub> )(Al <sub>0.216</sub> Mg <sub>2.475</sub> Fe <sup>3+</sup> <sub>0.226</sub> Fe <sup>2+</sup> <sub>0.028</sub> )O <sub>10</sub> (OH) <sub>2</sub>	40	38.07	0.70	41.01	1.40	37.16	0.91	3.85
Chlorite CCa-2 <sup>(4)</sup>	(Si <sub>2.633</sub> Al <sub>1.367</sub> )(Al <sub>1.116</sub> Mg <sub>2.964</sub> Fe <sup>3+</sup> <sub>0.215</sub> Fe <sup>2+</sup> <sub>1.712</sub> Ca <sub>0.011</sub> )O <sub>10</sub> (OH) <sub>8</sub>	40	46.49	0.90	56.01	1.30	55.93	-9.44	0.08

409 References: (1) Blanc et al. (2015) ; (2) Gailhanou et al. (2012) ; (3) Gailhanou et al. (2013); (4) Blanc et al. (2014); (5) Gaboreau et al. (2020)

410 <sup>a</sup>: log<sub>10</sub>K (298.15 K) differences between solubility and estimates411 <sup>b</sup>: log<sub>10</sub>K (298.15 K) differences between calorimetry and estimates

412

413

414

415

416 As illustrated in Figure 2, ClayTherm predictions are in very good agreement with the  
417 solubilities measured by Gaboreau et al. (2020). The relation is still correct with the  
418 equilibrium constants extracted from literature by Gaboreau et al. (2020), provided the set of  
419 data from Reesman (1974) is discarded (set A in Figure 2). The reason for discarding this  
420 dataset could lie in the unusually high liquid/solid ratio  $L/S = 200$  used by the authors, almost  
421 ten times higher than the ratio  $L/S=24$  used by Misra and Upchurch (1976) and Gaboreau et  
422 al. (2020). A high  $L/S$  ratio could delay the duration required to reach equilibrium and to  
423 overestimate the stability of the mineral. The last point strongly departs from the general  
424 tendency, point (3) in Figure 2, which corresponds to the equilibrium constant extracted by  
425 Huang and Keller (1973) for the Fithian illite. It is interesting to note that the analysis  
426 provided by the authors strongly differs from that provided by Reesman (1974). Furthermore,  
427 Huang and Keller (1973) do not explain the source of data for the mineral analyses, which  
428 could raise questions especially concerning the constant extracted for the Fithian Illite.  
429 Except for Reesman (1974) data and Huang and Keller (1973) Fithian illite data, all other  
430 constants are globally located within a  $\pm 2.0 \log_{10}K$  (298.15 K) interval. This interval is close  
431 to the  $\pm 1.7 \log_{10}K$  (298.15 K) previously deduced for the estimates, meaning that the  
432 estimated values are consistent with the solubility data selected from previous literature and  
433 displayed in Figure 2.  
434  
435  
436  
437

438  
439  
440

## 5. Calculation tool to derive illite/smectite compositions: ISTherm

441 A specific application and dedicated development are provided for the stability of  
442 illite/smectite interstratified minerals (I/S). Geloni et al. (2017) previously proposed a first  
443 application, based on Blanc et al. (2015), to estimate the thermodynamic properties of I/S  
444 minerals. This work introduces an evolution of the concept, integrating composition  
445 calculations and non-ideal mixing energies. Indeed, the goal of this second tool (ISTherm) is,  
446 from a given I/S composition, to derive the detailed composition of the smectite and illite end-  
447 members and intermediate compositions, according to the composition trend to which the I/S  
448 of interest belongs. ISTherm is a macro-enabled Microsoft Excel© file available upon  
449 request.

### 450 5.1. ILLITE/SMECTITE SOLID SOLUTION MODEL

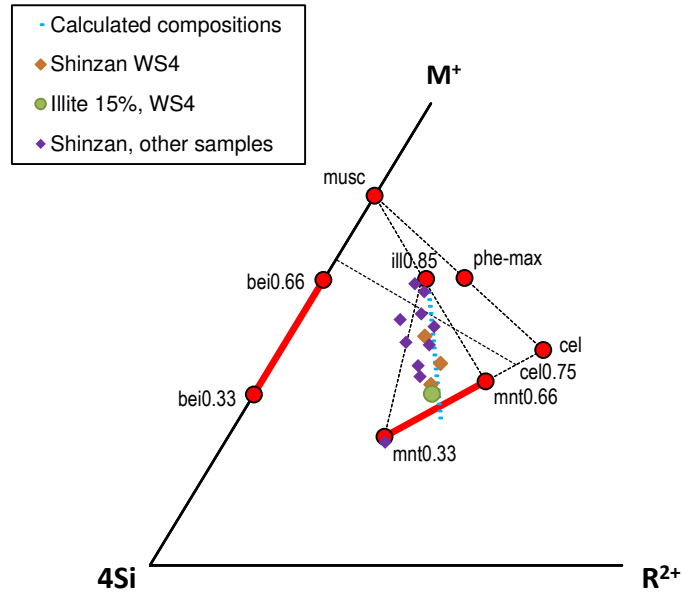
451 Gailhanou et al. (2019) reported the measurements of thermodynamic properties for an I/S  
452 mineral of given composition (ISCz-1, from the Source Clay repository). This measurement is  
453 used here to support the development and the verification of an I/S solid solution model and  
454 its implementation into a predicting tool.

#### 455 5.1.1. End-members composition calculation

456 According to Meunier and Velde (1989), the smectite-to-illite transformation reaction follows  
457 pre-determined composition trends. In particular, as shown in Figure 3, the I/S composition  
458 field has a triangular shape defined by a single illite end-member and two smectite end-  
459 members, which differ in the composition of the octahedral layer.

460  
461 Meunier and Velde (1989) showed that smectite composition evolves, with increasing  
462 temperature during diagenesis, from a compositional area lying along the Montmorillonite line  
463 (mnt0.33/mnt0.66, Figure 3), towards the Illite 0.85 end-member. This evolutionary path is  
464 recognizable as a linear trend within the trilinear space defined by the following end-  
465 members: (i) 4Si (the number of Si per  $O_{10}(OH)_2$ , divided by 4), (ii)  $R^{2+}$  (the number of  
466 octahedral divalent cations) and (iii)  $M^+$  (the total charge deficit). Despite this evidence, it is  
467 important to note that the three aforementioned parameters (4Si,  $R^{2+}$  and  $M^+$ ) cannot fully  
468 describe, in terms of interlayer cations ( $K^+$ ,  $Na^+$ ,  $Mg^{2+}$  or  $Ca^{2+}$ ), octahedral cations ( $Mg^{2+}$ ,  
469  $Fe^{2+}$ ,  $Fe^{3+}$ ,  $Al^{3+}$ ) or tetrahedral cations ( $Si^{4+}$  and  $Al^{3+}$ ), the complex composition of I/S  
470 minerals.

471  
472 The approach of Meunier and Velde (1989) was revisited by Meunier et al. (2004) for the  
473 presence of vermiculite layers in the stacking sequence of some I/S minerals. Such  
474 modifications can explain the increase in the tetrahedral charge for the montmorillonite  
475 component. These considerations are beyond the scope of the present work but they could  
476 be the focus of further developments for the model presented here.



477  
478 Figure 3 -  $4Si-R^{2+}-M^+$  projection displaying smectite-to-illite evolution trends, after Meunier  
479 and Velde, 1989.

480 Abbreviations: musc: muscovite; bei: beidellite; cel: celadonite; phe: phengite; mnt  
481 montmorillonite; ill: illite  
482  
483  
484

485 The calculation tool IStherm implements the approach developed by Meunier and Velde  
486 (1989) to calculate intermediate compositions along the trend joining the composition of the  
487 sample and the illite end member, up to the montmorillonite composition line (see Figure 3).  
488

489 The tool first calculates the composition of the illite and smectite end-members, based on  
490 their coordinates in the  $4Si-R^{2+}-M^+$  projection. Then, 20 intermediate compositions are  
491 determined, by increasing the illite content from the smectite end-member. The results of the  
492 calculation are illustrated in Figure 3 for the Shinzan I/S series (Gailhanou, 2005). The  
493 following points should be emphasized:

- 494 - The calculation implies that the number of octahedral cations is equal to that of the  
495 mineral composition considered, the same value for smectite and illite end-members  
496 and intermediate compositions;
- 497 - End-member coordinates in the  $4Si-R^{2+}-M^+$  projection determine the tetrahedral,  
498 octahedral and total layer charge. The tool calculates the linear variations of the  
499 charge between end-members and it provides the charge values for each of the  
500 intermediate compositions;
- 501 - Cations are distributed randomly among the different crystallographic sites;
- 502 - For sake of simplicity, the tool provides the possibility to replace Ti by Al and Mn by  
503 Mg.  
504

### 505 5.1.2. Thermodynamic properties of the solid solution

506 The thermodynamic properties of illite/smectite interstratified minerals have been  
507 investigated following three distinct approaches:

- 508
- 509 - by applying the global model implemented in ClayTherm to intermediate compositions  
510 corresponding to average values between the illite and smectite end-member;

- 511 - by considering a mechanical mixture of illite and smectite, i.e. by removing the energy
- 512 of mixing term from Equation (5);
- 513 - by considering a mechanical mixture that accounts for the energies of mixing (ideal +
- 514 non-ideal).

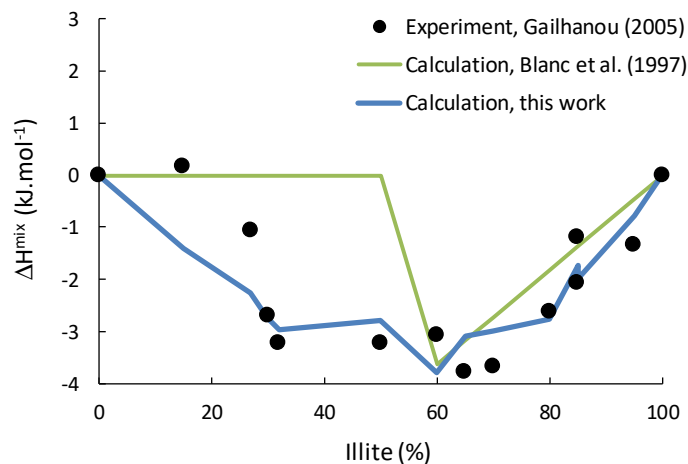
515  
 516 The results of the different approaches are discussed below, after an introductory section on  
 517 the calculation methods used to estimate the mixing properties.

518  
 519 The enthalpy of mixing  $\Delta H^{\text{mix}}$  can be directly obtained from the calorimetric measurements  
 520 performed on the I/S series from the Shinzan area by Gailhanou (2005) and Gailhanou et al.  
 521 (2019). These measurements are reported in Figure 4. A semi-empirical function was  
 522 developed to address  $\Delta H^{\text{mix}}$  variations with respect to smectite fraction  $X_{sm}$  in illite/smectite:

$$523 \Delta H^{\text{mix}} = x_{sm} \cdot (36.01 \cdot x_{sm} \cdot R^{2+} - 19.03) \quad (13)$$

524  
 525  
 526 This function not only depends on the smectite fraction (as expected for an illite/smectite  
 527 interaction term) but it also includes an octahedral composition dependence, to account for  
 528 the variability observed for the Shinzan samples (Gailhanou, 2005). For comparison, the  
 529 results provided using the solid solution model developed by Blanc et al. (1997) are also  
 530 displayed (Figure 4). This model includes short range ordering and was parameterized  
 531 considering diagenetic illite/smectite series. The results are similar to the measurements, at  
 532 least for R1 ordered I/S samples (illite > 55 to 60 %). For the smectite-rich minerals, Blanc et  
 533 al. (1997) considered that the disordered I/S stacking sequence implied  $\Delta H^{\text{mix}} = 0 \text{ J} \cdot \text{mol}^{-1}$ .  
 534 This statement is wrong, given the experiment results displayed in Figure 4. In this work, the  
 535 function from Equation (13) is complemented with an ideal entropy of mixing term, as in  
 536 Equation (7), to calculate the Gibbs energy of mixing used in Figure 5. This choice allows  
 537 quite a simple hypothesis to be tested, knowing that more complex expressions have been  
 538 developed, especially to include the influence of ordering in the expression of the entropy of  
 539 mixing (Blanc et al., 1997).

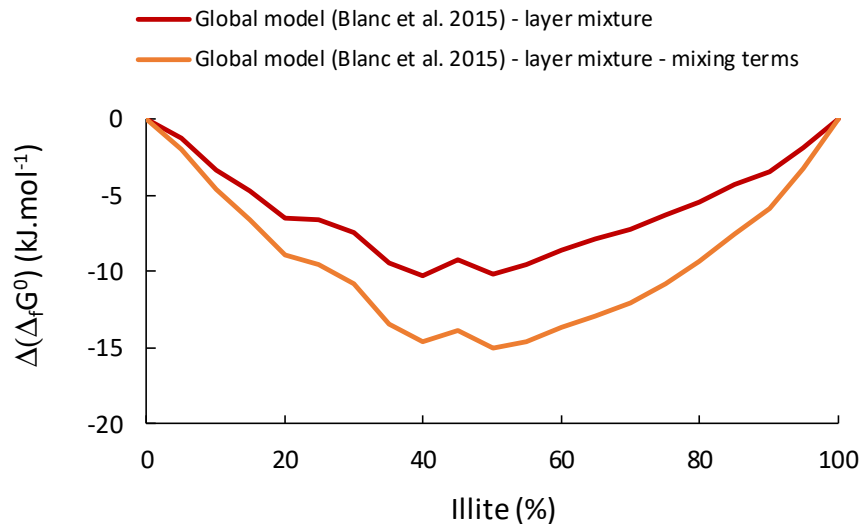
540  
 541  
 542



543  
 544 *Figure 4 – Enthalpies of mixing determined for Shinzan series of samples from Gailhanou*  
 545 *(2005) measurements*  
 546  
 547

548 Figure 5 illustrates the differences, in terms of Gibbs energy ( $\Delta G^{\text{mix}}$ ), between the three  
 549 different methods used to estimate I/S thermodynamic properties, i.e. the global model  
 550 (ClayTherm), the mechanical mixture and the non-ideal mixture. The curves displayed in  
 551 Figure 5 correspond to the Gibbs energy differences between the global model and the

552 mechanical mixture or the non-ideal mixture models, respectively. I/S compositions  
553 correspond to samples from the Shinzan series studied by Gailhanou (2005) and Gailhanou  
554 et al. (2019). Since the differences are globally negative, it implies that the mixture of illite  
555 and smectite layers stabilizes I/S of intermediate composition. This effect is enhanced when  
556 considering the mixing terms in the solid solution model, consistently with the negative  
557 enthalpies of mixing measured by Gailhanou (2005) and Gailhanou et al. (2019) and  
558 displayed in Figure 4.  
559  
560  
561  
562



563  
564 Figure 5 – Estimates of illite/smectite Gibbs free energy of mixing for Shinzan series  
565 (composition of samples after Gailhanou et al., 2019).  
566

567  
568  
569 Similar calculations were performed by Gailhanou et al. (2019) for the ISCz-1 sample. The  
570  $\Delta_f G^0$  estimated by the authors is also closest to the experiment values ( $\Delta < 0.01$  %) when  
571 non-ideal mixture of illite and smectite layers is considered. In addition, ISCz-1 disappears  
572 from the stable phases when  $\Delta_f G^0$  is estimated using the global model. It re-appears among  
573 the stable phases when considering a non-ideal mixture of illite and smectite layers for the  
574  $\Delta_f G^0$  estimate calculation. This comparison enforces the use of the non-ideal model for I/S  
575 estimates.  
576  
577

## 579 **5.2. APPLICATION TO THE SHINZAN SERIES CASE**

580 A series of fourteen illite-smectite mixed-layer samples taken from the Shinzan area,  
581 northeast Japan, was also used for this study. This series, well described in the literature  
582 (Inoue et al., 1987; Inoue and Utada, 1983), is noticeable as it consists in a complete mixed-  
583 layer series with chemical compositions varying from montmorillonite to illite end-members.  
584 The series results from the hydrothermal alteration of dioctahedral micas/smectites. The  
585 continuous conversion of smectite into illite has been described by Inoue et al. (1987). The  
586 main transformation mechanism suggested by the authors was based on the dissolution of  
587 smectite and the crystallization of illite. A solid-state transformation mechanism was also  
588 shown from HRTEM observations (Amouric and Olives, 1991; Olives et al., 2000).  
589

### 590 **5.2.1. Stability diagrams for the WS4 Shinzan series**

591 Considering the full composition of a sample from the WS4 borehole (sample B in Gailhanou  
592 2005), the calculation tool is used in order to calculate the composition and thermodynamic  
593 properties of a series of 10 I/S with an amount of illite ranging from 0% (pure smectite) to  
594 100% (pure illite). This series was selected because it displays a central location in the illite-  
595 mnt0.33-mnt0.66 triangle (see Figure 3). These compositions are reported in Figure 2,  
596 together with the fourteen samples from the Shinzan area analysed by Gailhanou (2005).  
597 The thermodynamic properties and detailed composition of the samples are presented in  
598 Annex 1 (supplementary data). The stability fields of each I/S composition are represented in  
599 Figure 6A to D, at 25 and 150°C, for anhydrous and hydrated I/S phases. Figures 6 also  
600 present the solution compositions collected by Aagaard and Helgeson (1983) and used by  
601 Aagaard and Helgeson (1983) and Garrels (1984) to illustrate the illite/smectite stability  
602 fields. I/S phases are supplemented to the original Aagaard and Helgeson (1983) legend, in  
603 agreement with the discussion presented by the authors. The agreement between the  
604 mineralogical assemblage in contact with solutions and the stability fields is globally correct  
605 for Figure 6.D, drawn at 25°C for hydrated I/S phases. This corresponds to the subsurface  
606 condition of water sampling, in the studies selected by Aagaard and Helgeson (1983). At  
607 25°C (Figure 6.B), the stability field of anhydrous I/S phases is globally shifted toward the  
608 high silica activities, which is not in agreement with the location of the solutions in contact  
609 with mineral assemblages including montmorillonite. At higher temperatures (Figures 6.A and  
610 6.C), differences between anhydrous and hydrated I/S are more limited, consistently with the  
611 decrease of I/S in the clay water when the smectite fraction decreases. From Figures 6.A  
612 and 6.C, a temperature increase induces the displacement of the stability fields toward the  
613 high silica activities, which stabilizes illite-rich I/S compositions, consistently with the I/S  
614 composition evolution during diagenesis (Velde and Vasseur, 1992). This effect would even  
615 be reinforced by the transition from Opal-A to Opal-CT to quartz, occurring in early diagenetic  
616 sequences (Compton, 1991), over long periods of time and a temperature rise, which would  
617 naturally decrease the silica activity.

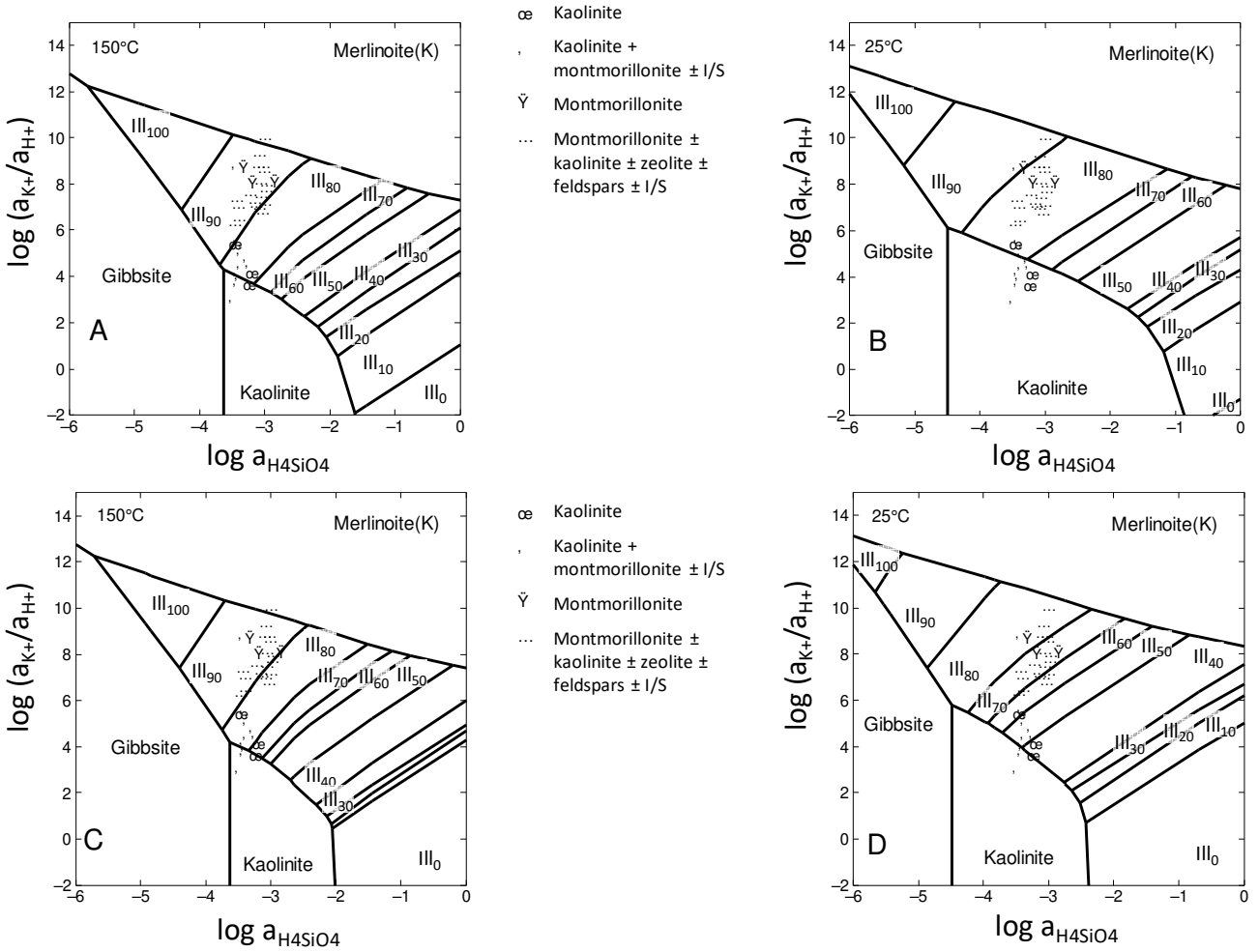
618

619

620

621

622  
623



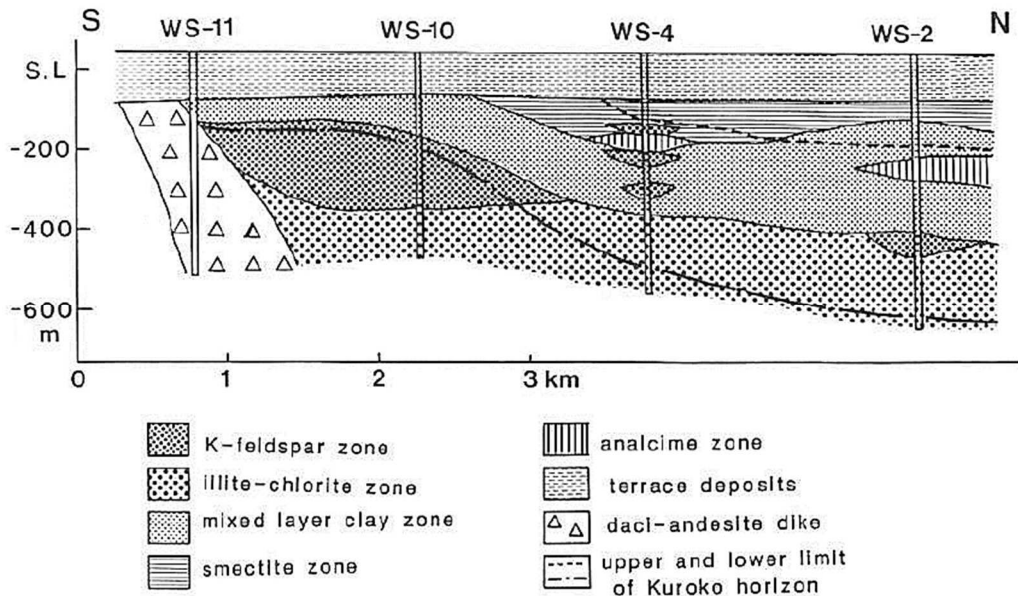
624  
625  
626  
627  
628  
629  
630

Figure 6 – I/S stability fields calculated for the WS4 Shinzan series, anhydrous phases: A) at 150°C, B) at 25°C; hydrated phases: C) at 150°C, D) at 25°C  
 Concentrations of elements other than Si, K or Al are established by stating the equilibrium with the following minerals: anorthite (Ca), albite (Na), lizardite (Mg), magnetite and ferrihydrite (Fe and dissolved O<sub>2</sub>)

### 632 5.2.2. Reactive transport modelling: case of the WS4 Shinzan series

633 This section presents a case of preliminary reactive transport calculation for the WS4  
 634 Shinzan geothermal borehole (Shinzan area, Akita Prefecture, Northeast Japan). The  
 635 calculation aims to reproduce the progressive illitization of a smectite-rich formation, altered  
 636 by a geothermal hot fluid. These calculations imply different hypotheses for the geological  
 637 formation and the hydrothermal fluids, which rely on previous literature observations and  
 638 measurements. Lacking compositions or parameters were addressed by analogy with similar  
 639 contexts. This exercise highlights the potential and some weaknesses for illitization  
 640 geochemical modelling, based on the developments presented in this work.

641  
 642 The Shinzan area, covered by quaternary sediments, presents two pyroclastic Miocene  
 643 formations, which have been subjected to hydrothermal alteration. A vertical cross-section  
 644 representing the Shinzan geothermal field with the main boreholes is given in Figure 7.  
 645



646  
 647

648 Figure 7 – Distribution of the mineral zones in the Shinzan field (after Inoue et al. (1992))

649  
 650

#### 651 **Initial materials and fluids**

652

653 The composition of the geothermal fluid proposed by Inoue and Utada (1983) is given in  
 654 Table 3. The fluid chemistry considered in calculations was established by processing a first  
 655 geochemical calculation, assuming a temperature of 220°C, based on the work published by  
 656 Inoue et al. (1992) (Figure 6 in Inoue et al., 1992). In this calculation, thermodynamic  
 657 equilibrium is assumed between the solution and a mineralogical assemblage made of  
 658 quartz, pure illite and gibbsite, in order to constrain Si, Mg and Al concentrations, i.e.  
 659 concentrations not or roughly estimated by Inoue and Udata (1983). A CO<sub>2</sub> partial pressure  
 660 of 0.1 bar was considered, typical of underground environments (Coudrain-Ribstein et al.,  
 661 1998).

662

663 The compositions and thermodynamic properties of an I/S series was calculated using  
 664 ISTherm, based on sample B from the WS4 series (Gailhanou, 2005), as reported in the  
 665 previous section. For the present calculation, only anhydrous minerals were considered, for  
 666 sake of simplicity and because the difference, in terms of stability, between hydrated and

667 anhydrous minerals is lower at high temperature (Figures 6.A and 6.C). A calculation case  
 668 using hydrated compositions showed no significant differences with the results reported here.  
 669 The composition of the I/S minerals is represented in Figure 3, their thermodynamic  
 670 properties are provided in Annex 1 and their stability fields are reported in Figure 6.

671  
 672 The works published by Inoue and Utada (1983) and Inoue et al. (1987, 1992) on the  
 673 Shinzan claystone focus on the smectite-to-illite conversion. Limited information is provided  
 674 concerning accessory minerals. For the smectite-rich formation, a simple assumption is  
 675 considered with pure smectite as the starting material, with traces of gibbsite and quartz, to  
 676 help control dissolved silica and alumina in the first steps of the reaction. A porosity of 20 %  
 677 was also arbitrarily considered.

678  
 679

680 Table 3 - *Composition of the geothermal fluid and associated mineralogy (in mol.L<sup>-1</sup>).*

	Hydrothermal fluid		Initial formation
	Inoue and Utada (1983)	This study	Fluid
T (°C)	250 ± 50°C	220°C	195°C
pH	4.5 ± 0.5 at 25°C	4.6 at 220°C	7.0 at 195°C
Cl	0.89	0.99	0.84
Na	0.85	0.85	0.86
K	0.11	0.11	3.6 10 <sup>-10</sup>
Ca	1.3 10 <sup>-2</sup>	1.3 10 <sup>-2</sup>	1.8 10 <sup>-9</sup>
Mg	0.4 to 4.3 10 <sup>-4</sup>	4.3 10 <sup>-4</sup>	1.1 10 <sup>-8</sup>
SO <sub>4</sub>	3.3 10 <sup>-9</sup>	3.3 10 <sup>-9</sup>	1.2 10 <sup>-3</sup>
Al	--	2.3 10 <sup>-5</sup>	5.0 10 <sup>-3</sup>
Si	--	6.5 10 <sup>-3</sup>	195°C
C(4)	--	7.8 10 <sup>-4</sup>	--
Fe	--	--	4.2 10 <sup>-9</sup>
Smectite			30
Quartz			1
Gibbsite			1
Porosity			0.2

681  
 682  
 683 To our knowledge, smectite porewater has not been analysed. A hypothetical fluid  
 684 composition was calculated (Table 3: Initial formation) assuming equilibrium with respect to  
 685 pure smectite (composition given in Annex 1), quartz and gibbsite and considering the same  
 686 Na concentration as that of the geothermal fluid.

687  
 688

### 689 **Conceptual model**

690 The modelling was based on a 1D column representing the vertical profile of the WS4  
 691 borehole. The profile consisted in 100 m of smectite, discretized into 100 cells of 1 m (see  
 692 Figure 8). A linear temperature gradient from 220°C (inlet of the geothermal fluid) to 170°C  
 693 (outlet of the geothermal fluid) was imposed, based on Inoue et al. (1992). A flowrate of 0.05  
 694 m year<sup>-1</sup> was considered. The I/S compositions and thermodynamic properties are given in  
 695 Annex 1. Geochemical calculations were performed using the code PhreeqC (Parkhurst and  
 696 Appelo, 2013) and the thermodynamic database Thermoddem (Blanc et al., 2012), enriched  
 697 with thermodynamic data established here (see Table A1 in Annex 1).  
 698

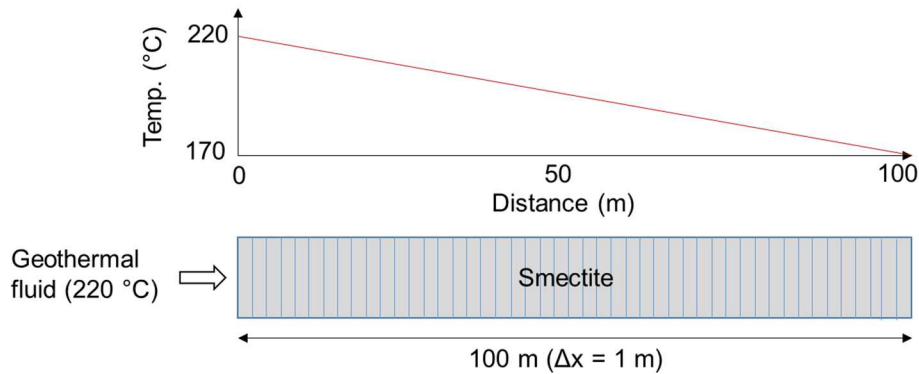


Figure 8 - Discretized profile for the Shinzan WS4 borehole modelling.

699  
700  
701  
702  
703  
704  
705  
706  
707  
708  
709  
710  
711  
712  
713  
714  
715  
716  
717  
718  
719  
720  
721  
722  
723  
724  
725  
726  
727  
728  
729  
730  
731  
732  
733  
734  
735  
736  
737  
738  
739  
740

### Results

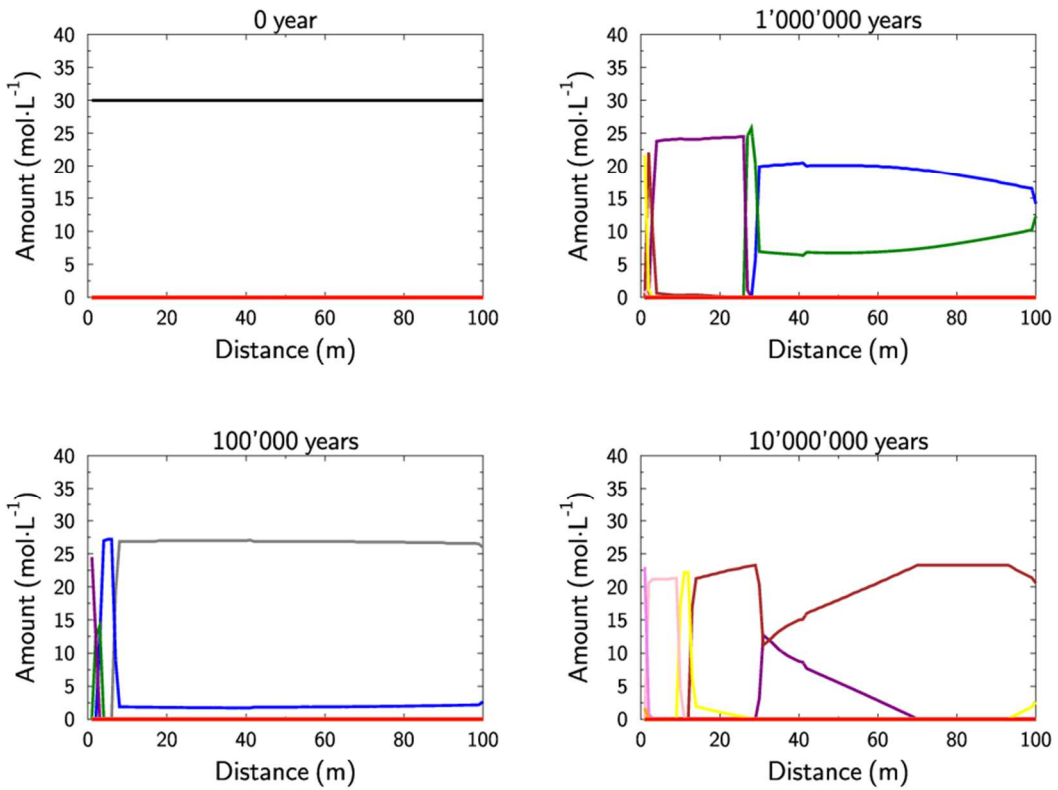
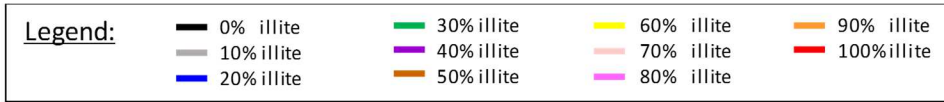
Modelling results are reported in Figures 9, 10 and 11. Figure 9 shows the evolution of the smectite composition, revealing an efficient smectite-to-illite conversion up to the formation of an I/S with 80% illite after 10 Ma reaction time. As expected, the most relevant mineralogical transformation predicted by the numerical model is the pervasive illitization of the original rock, indicated by an augmented percentage of the illitic term in the I/S. The following sequence is obtained: from pure smectite to 10, 20, 30, 40, 50, 60, 70 and finally 80% illite after 10 Ma reaction time.

Another relevant feature of the mineralogical reworking predicted by the model is the concomitant precipitation of gibbsite and quartz. The occurrence of quartz (Figure 10) in our model is consistent with previous observations (Herman and Lahan, 1981) about the precipitation of quartz during the illitization of smectite, according to the scheme:



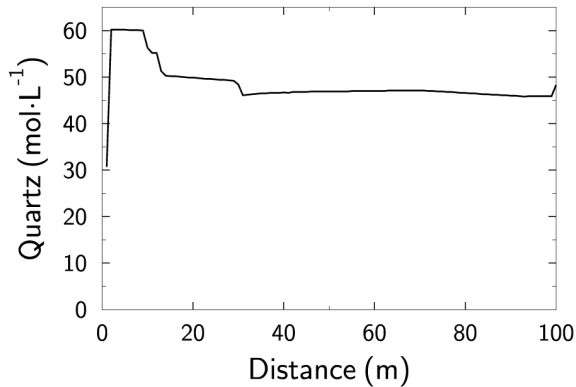
The porewater chemistry simulated after 10 Ma is shown in Figure 11. Contact with geothermal fluid led to acidic conditions between 0 and 10 m. The Si concentration decreased linearly from 0 to 100 m, consistent with the quartz equilibrium condition imposed under the fixed, linear temperature gradient of Figure 8. The Na concentration was constant during the entire simulation, and K concentrations remained quite unchanged over the first 100 m of the modelled domain (i.e.  $\sim 0.108 \text{ mol L}^{-1}$ ), in spite of the concomitant extensive illitization of the smectite fraction. The formation of illite-rich I/S phases was driven by high concentrations of aqueous Al.

Noteworthy, the smectite-to-illite transformation predicted by the model is consistent with the Miocene age of the formation documented by Inoue and Utada (1983). We consider the overall agreement between numerical results and field observations as an argument for the correctness of the thermodynamic properties predicted for the illite/smectite minerals of interest, and for the potential of our estimation tool. The geochemical model could be improved by including kinetically controlled reactions, like the Opal-A to Quartz transformation and potassium fixation, as a first step towards smectite illitization.



741  
742  
743  
744  
745

Figure 9 – Modelling of the evolution of I/S composition during smectite hydrothermal transformation.



746  
747  
748  
749  
750  
751  
752  
753  
754  
755  
756  
757

Figure 10 - Modelled quartz profile after 10 Ma reaction time

758  
759

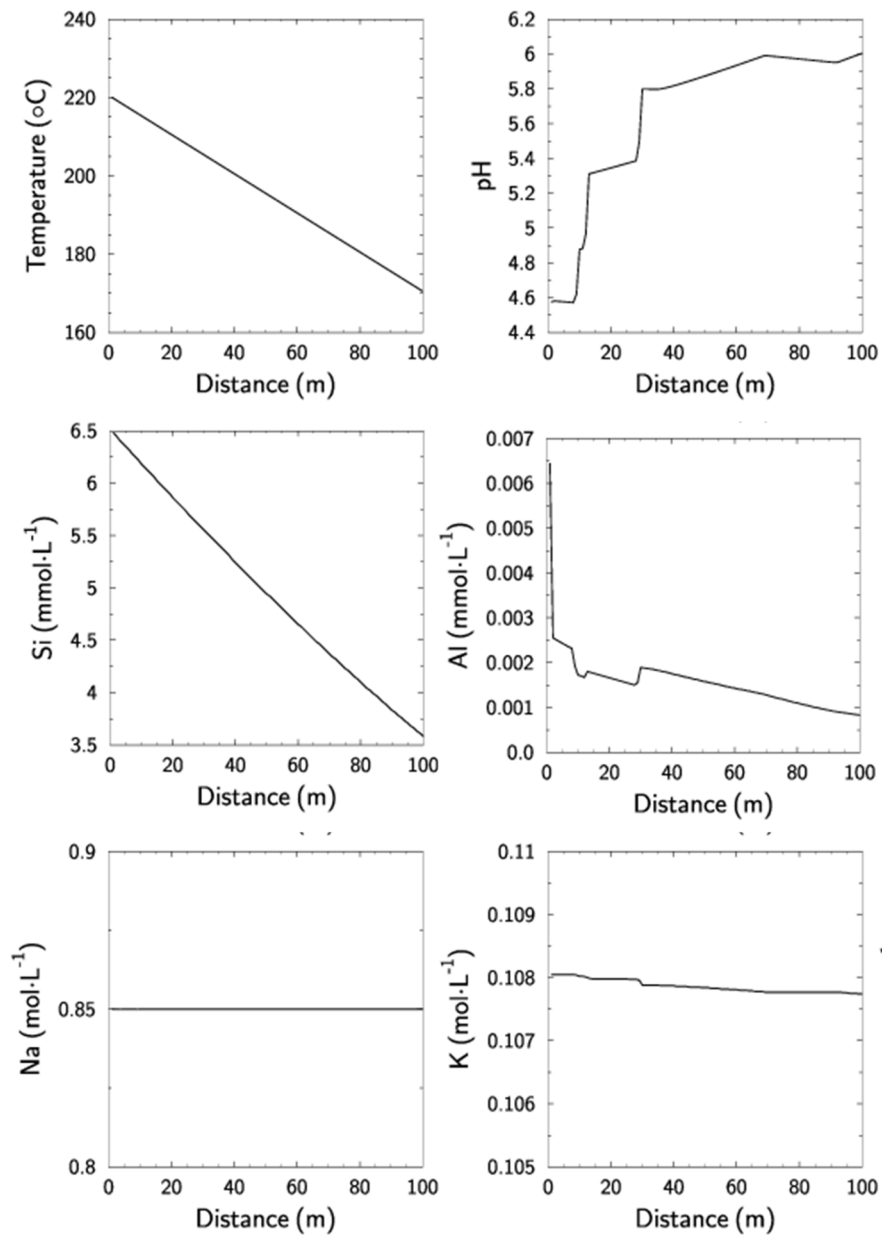


Figure 11 - Porewater chemistry after 10 Ma reaction time

760  
761  
762  
763

## 6. Concluding remarks

765 We document the development of two calculation tools, ClayTherm and ISTherm, devoted to  
766 the estimation of the thermodynamic properties of clay minerals. These tools are aimed at  
767 combining pre-existing estimation models in new applications for their easy use in a  
768 potentially wider scientific community. Further to this, ClayTherm and ISTherm have the  
769 capability to model both anhydrous and hydrated phases more accurately than the models  
770 from which they derive.

771  
772 The first estimation tool, ClayTherm, was developed by taking advantage of the estimation  
773 models previously fine-tuned by Blanc et al. (2015), Gailhanou et al. (2017) and Vieillard et  
774 al. (2019). Compared to these previous models, ClayTherm represents a refinement in the  
775 description of cation sharing among the crystallographic sites. The verification of the model  
776 was carried out by comparison of the numerical outputs with solubility data recently  
777 published by Gaboreau et al. (2020) and archived in the datasets selected by these authors  
778 from previous literature. ClayTherm estimations are in good agreement with data from the  
779 literature, calorimetry data included, except for chlorite, which was not found to reach  
780 equilibrium in solubility experiments. Some discrepancies between estimated and measured  
781 data were observed for vermiculite, possibly because of the presence of organic carbon in  
782 the sample measured by Gailhanou et al. (2013).

783  
784 Directly derived from ClayTherm, the second estimation tool, ISTherm, is specifically  
785 designed to investigate the thermodynamic properties of interstratified illite/smectite minerals.  
786 In particular, it allows for the calculation of the thermodynamic properties of a series of  
787 illite/smectite (I/S) minerals from the composition of the smectitic and illitic end-members,  
788 and from a single I/S composition. The thermodynamic functions implemented in ISTherm,  
789 account for the specific contribution of the mixing energies term. The tool was used to  
790 investigate a natural I/S series from the Shinzan hydrothermal area, Japan. The results  
791 indicate that both temperature and hydration are first-order controlling parameters of the  
792 shape and extension of the illite/smectite stability fields. In particular, predominance stability  
793 fields of smectite-rich phases tend to increase when hydration is correctly accounted for in  
794 equilibrium reactions, whereas higher temperatures tend to displace the stability field of illite-  
795 rich phases towards higher activity values of dissolved silica.

796  
797 The correctness of the estimated thermodynamic data was indirectly tested by a reactive  
798 transport modelling approach. Simplified, prototypical models were run to reproduce the  
799 hydrothermal alteration patterns observed in the Shinzan geothermal area, Japan. The  
800 formation of intermediate I/S phases during the illitization of smectite was successfully  
801 modelled, in agreement with site-specific mineralogical observations.

802  
803

804

### ACKNOWLEDGEMENTS

805 Financial support from the Thermochimie projects TempaSiamK (n° 20071653 CGK) and  
806 Domhyne (20081010 COX) and from the Stab-Inter BRGM/IGG project are gratefully  
807 acknowledged. Exchanges and contributions from Arnault Lassin, Mathieu Debure and  
808 Francis Claret at BRGM and Claire Fialips from Total were particularly helpful to us and  
809 welcomed. The whole project could not be completed without the contributions of colleagues  
810 from Marseille (IM2NP: Jacques Rogez and Georges Mikaelian, MADIREL: Renaud Denoyel  
811 and Emily Bloch) and from Tokyo (TOKYOTECH: Hitoshi Kawaji), we are very grateful to  
812 them. This article is especially dedicated to the late Eric Giffaut, whose talent and constant  
813 efforts were decisive in achieving this 17-year suite of scientific programs.

814

815  
816

## 7. References

817  
818

- 819 Aagaard, P., Helgeson, H.C., 1983. Activity/composition relations among silicates and  
820 aqueous solutions: II. Chemical and thermodynamic consequences of ideal mixing of atoms  
821 on homological sites in montmorillonites, illites, and mixed-layer clays. *Clays and Clay*  
822 *Minerals* 31, 207-217.
- 823 Aja, S.U., Rosenberg, P.E., Kittrick, J.A., 1991. Illite equilibria in solutions: I. Phase  
824 relationships in the system  $K_2O-Al_2O_3-SiO_2-H_2O$  between 25 and 250°C. *Geochimica et*  
825 *Cosmochimica Acta* 55, 1353-1364.
- 826 Amouric, M., Olives, J., 1991. Illitization of smectite as seen by high-resolution transmission  
827 electron microscopy. *European Journal of Mineralogy* 3, 831-835.
- 828 Battaglia, S., Gherardi, F., Gianelli, G., Leoni, L., Lezzerini, M., 2013. Alteration of clay  
829 minerals in a sedimentary caprock and its use in geothermal prospecting: an example from  
830 Mt. Amiata. *Clay Minerals* 48, 37-58.
- 831 Benson, S.W., 1968. Thermochemical kinetics: methods for the estimation of  
832 thermochemical data and rate parameters. Wiley.
- 833 Bertoldi, C., Dachs, E., Cemic, L., Theye, T., Wirth, R., Groger, W., 2005. The heat capacity  
834 of the serpentine subgroup mineral berthierine  $(Fe_{2.5}Al_{0.5})[Si_{1.5}Al_{0.5}O_5](OH)_4$ . *Clays and Clay*  
835 *Minerals* 53, 380-388.
- 836 Blanc, P., Bieber, A., Fritz, B., Duplay, J., 1997. A short range interaction model applied to  
837 illite/smectite mixed-layer minerals. *Physics and Chemistry of Minerals* 24, 574-581.
- 838 Blanc, P., Gailhanou, H., Rogez, J., Mikaelian, G., Kawaji, H., Warmont, F., Gaboreau, S.,  
839 Grangeon, S., Grenèche, J.-M., Vieillard, P., Fialips, C.I., Giffaut, E., Gaucher, E.C., Claret,  
840 F., 2014. Thermodynamic properties of chlorite and berthierine derived from calorimetric  
841 measurements. *Physics and Chemistry of Minerals* 41, 603-615.
- 842 Blanc, P., Lassin, A., Piantone, P., Azaroual, M., Jacquemet, N., Fabbri, A., Gaucher, E.C.,  
843 2012. Thermoddem: A geochemical database focused on low temperature water/rock  
844 interactions and waste materials. *Applied Geochemistry* 27, 2107-2116.
- 845 Blanc, P., Vieillard, P., Gailhanou, H., Gaboreau, S., Gaucher, E.C., Fialips, C.I., Madé, B.,  
846 Giffaut, E., 2015. A generalized model for predicting the thermodynamic properties of clay  
847 minerals. *American Journal of Science* 315, 734-780.
- 848 Brown, G., 1982. Crystal structures of clay minerals and their X-ray identification. The  
849 Mineralogical Society of Great Britain and Ireland.
- 850 Chermak, J.A., Rimstidt, J.D., 1989. Estimating the thermodynamic properties ( $\Delta G^{\circ}$  and  
851  $\Delta H^{\circ}$ ) of silicate minerals at 298 K from the sum of polyhedral contributions. *American*  
852 *Mineralogist* 74, 1023-1031.

- 853 Circone, S., Navrotsky, A., 1992. Substitution of <sup>[6,4]Al</sup> in phlogopite; high-temperature  
854 solution calorimetry, heat capacities, and thermodynamic properties of the phlogopite-  
855 eastonite join. *American Mineralogist* 77, 1191-1205.
- 856 Compton, J.S., 1991. Origin and diagenesis of clay minerals in the Monterey Formation,  
857 Santa Maria Basin Area, California. *Clays and Clay Minerals* 39, 449-466.
- 858 Coudrain-Ribstein, A., Gouze, P., de Marsily, G., 1998. Temperature-carbon dioxide partial  
859 pressure trends in confined aquifers. *Chemical Geology* 145, 73-89.
- 860 Cox, J.D., Wagman, D.D., Medvedev, V.A., 1989. CODATA key values for thermodynamics.  
861 Hemisphere Pub. Corp.
- 862 Dachs, E., Benisek, A., 2019. A new activity model for Mg–Al biotites determined through an  
863 integrated approach. *Contributions to Mineralogy and Petrology* 174, 76.
- 864 Dubacq, B., Vidal, O., Andrade, V.D., 2010. Dehydration of dioctahedral aluminous  
865 phyllosilicates: thermodynamic modelling and implications for thermobarometric estimates.  
866 *Contributions to Mineralogy and Petrology* 159, 159-174.
- 867 Essene, E.J., Peacor, D.R., 1995. Clay mineral thermometry; a critical perspective. *Clays  
868 and Clay Minerals* 43, 540-553.
- 869 Gaboreau, S., Gailhanou, H., Blanc, P., Vieillard, P., Made, B., 2020. Clay mineral solubility  
870 from aqueous equilibrium: Assessment of the measured thermodynamic properties. *Applied  
871 Geochemistry* 113, 104465.
- 872 Gailhanou, H., 2005. Détermination expérimentale des propriétés thermodynamiques et  
873 étude des nanostructures de minéraux argileux. *Aix-Marseille* 3, p. 262.
- 874 Gailhanou, H., Blanc, P., Rogez, J., Mikaelian, G., Horiuchi, K., Yamamura, Y., Saito, K.,  
875 Kawaji, H., Warmont, F., Grenèche, J.-M., Vieillard, P., Fialips, C.I., Giffaut, E., Gaucher,  
876 E.C., 2013. Thermodynamic properties of saponite, nontronite, and vermiculite derived from  
877 calorimetric measurements. *American Mineralogist* 98, 1834-1847.
- 878 Gailhanou, H., Blanc, P., Rogez, J., Mikaelian, G., Kawaji, H., Olives, J., Amouric, M.,  
879 Denoyel, R., S., B., Montouillout, V., Vieillard, P., Fialips, C.I., Giffaut, E., Michau, N.,  
880 Gaucher, E.C., 2012. Thermodynamic properties of illite IMt-2, smectite MX-80 and beidellite  
881 SBld-1 by calorimetric methods: Enthalpies of formation, heat capacities, entropies and  
882 Gibbs free energies of formation. *Geochimica Cosmochimica Acta* 89, 279-301.
- 883 Gailhanou, H., Blanc, P., Rogez, J., Mikaelian, G., Kawaji, H., Olives, J., Montouillout, V.,  
884 Grenèche, J.M., Vieillard, P., Gaucher, E.C., Fialips, C.I., Madé, B., 2019. Thermodynamic  
885 properties of mixed-layer illite-smectite by calorimetric methods: Acquisition of the enthalpies  
886 of mixing of illite and smectite layers. *The Journal of Chemical Thermodynamics* 138, 78-97.
- 887 Gailhanou, H., Rogez, J., Miltenburg, J.C.v., Genderen, A.C.G.v., Grenèche, J.M., Gilles, C.,  
888 Jalabert, D., Michau, N., Gaucher, E.C., Blanc, P., 2009. Thermodynamic properties of  
889 chlorite CCa-2. Heat capacities, heat contents and entropies. *Geochimica et Cosmochimica  
890 Acta* 73, 4738-4749.
- 891 Gailhanou, H., van Miltenburg, J.C., Rogez, J., Olives, J., Amouric, M., Gaucher, E.C., Blanc,  
892 P., 2007. Thermodynamic properties of anhydrous smectite MX-80, illite IMt-2 and mixed-  
893 layer illite–smectite ISCz-1 as determined by calorimetric methods. Part I: Heat capacities,  
894 heat contents and entropies. *Geochimica et Cosmochimica Acta* 71, 5463-5473.

- 895 Gailhanou, H., Vieillard, P., Blanc, P., Lassin, A., Denoyel, R., Bloch, E., De Weireld, G.,  
896 Gaboreau, S., Fialips, C.I., Madé, B., Giffaut, E., 2017. Methodology for determining the  
897 thermodynamic properties of smectite hydration. *Applied Geochemistry* 82, 146-163.
- 898 Garrels, R.M., 1984. Montmorillonite/illite stability diagrams. *Clays and Clay minerals* 32,  
899 161-166.
- 900 Gaucher, E.C., Tournassat, C., Pearson, F.J., Blanc, P., Crouzet, C., Lerouge, C., Altmann,  
901 S., 2009. A robust model for pore-water chemistry of clayrock. *Geochimica et Cosmochimica*  
902 *Acta* 73, 6470-6487.
- 903 Geloni, C., Previde Massara, E., Di Paola, E., Ortenzi, A., Blanc, P., Gherardi, F., 2017.  
904 Modelling clay diagenesis using a combined crystal chemistry and thermochemistry  
905 approach: a case study on smectite illitization. *Energy Procedia* 125, 630-639.
- 906 Gherardi, F., Audigane, P., 2014. Geochemical reactivity in CO<sub>2</sub> geological storage sites.  
907 *Greenhouse Gas Sci Technol* 4, 157-159.
- 908 Giffaut, E., Grivé, M., Blanc, P., Vieillard, P., Colàs, E., Gailhanou, H., Gaboreau, S., Marty,  
909 N., Madé, B., Duro, L., 2014. ANDRA thermodynamic database for performance  
910 assessment: ThermoChimie. *Applied Geochemistry* 49, 225-236.
- 911 Helgeson, H., Delany, J., Nesbitt, H., Bird, D., 1978. Summary and critique of the  
912 thermodynamic properties of rock-forming minerals. *American Journal of Science* 278, 1-229.
- 913 Hemingway, B.S., Robie, R.A., Kittrick, J.A., Grew, E.S., Nelen, J.A., London, D., 1984. The  
914 heat capacities of osumilite from 298.15 to 1000 K, the thermodynamic properties of two  
915 natural chlorites to 500 K, and the thermodynamic properties of petalite to 1800 K. *United*  
916 *States Geological Survey*, pp. 701-710.
- 917 Herman, R.E., Lahan, R.W., 1981. Smectite to illite conversion rates: effects of solution  
918 chemistry. *Clays and Clay Minerals* 29, 129-135.
- 919 Holland, T.J.B., 1989. Dependence of entropy on volume for silicate and oxide minerals. A  
920 review and a prediction model. *American Mineralogist*, 74, 5-13.
- 921 Holland, T.J.B., Powell, R., 1998. An internally consistent thermodynamic data set for phases  
922 of petrological interest. *Journal of Metamorphic Geology* 16, 309-343.
- 923 Hower, J., Mowatt, T.C., 1966. The mineralogy of illites and mixed-layer illite/  
924 montmorillonites. *American Mineralogist* 51, 825-854.
- 925 Huang, W.H., Keller, W.D., 1973. Gibbs free energy of formation calculated from dissolution  
926 data using specific mineral analyses. *American Mineralogist* 58, 1023-1028.
- 927 Inoue, A., 1983. Potassium fixation by clay minerals during hydrothermal treatment. *Clays*  
928 *and Clay Minerals* 31, 81-91.
- 929 Inoue, A., Kohyama, N., Kitagawa, R., Watanabe, T., 1987. Chemical and morphological  
930 evidence for the conversion of smectite to illite. *Clays and Clay Minerals* 35, 111-120.
- 931 Inoue, A., Utada, M., 1983. Further Investigations of a conversion series of dioctahedral  
932 mica/smectites in the Shinzan hydrothermal alteration area, northeast Japan. *Clays and Clay*  
933 *Minerals* 31, 401-412.

- 934 Inoue, A., Utada, M., Wakita, K., 1992. Smectite-to-illite conversion in natural hydrothermal  
935 systems. *Applied Clay Science* 7, 131-145.
- 936 Kittrick, J.A., 1984. Solubility measurements of phases in three illites. *Clays and Clay*  
937 *Minerals* 32, 115-124.
- 938 Kittrick, J.A., Peryea, F.J., 1988. Experimental validation of the monophasic structure model  
939 for montmorillonite solubility. *Soil Science Society of America Journal* 52, 1199-1201.
- 940 Landais, P., 2006. Advances in geochemical research for the underground disposal of high-  
941 level, long-lived radioactive waste in a clay formation. *Journal of Geochemical Exploration*  
942 88, 32-36.
- 943 Marty, N.C.M., Tournassat, C., Burnol, A., Giffaut, E., Gaucher, E.C., 2009. Influence of  
944 reaction kinetics and mesh refinement on the numerical modelling of concrete/clay  
945 interactions. *Journal of Hydrology* 364, 58-72.
- 946 May, H.M., Klennburgh, D.G., Helmke, P.A., Jackson, M.L., 1986. Aqueous dissolution,  
947 solubilities and thermodynamic stabilities of common aluminosilicate clay minerals: Kaolinite  
948 and smectites. *Geochimica et Cosmochimica Acta* 50, 1667-1677.
- 949 Meunier, A., Lanson, B., Velde, B., 2004. Composition variation of illite-vermiculite-smectite  
950 mixed-layer minerals in a bentonite bed from Charente (France). *Clay Minerals* 39, 317-332.
- 951 Meunier, A., Velde, B., 1989. Solid solutions in I/S mixed-layer minerals and illite. *American*  
952 *Mineralogist* 74, 1106-1112.
- 953 Meunier, A., Velde, B., Griffault, L., 1998. The reactivity of bentonites: A review. An  
954 application to clay barrier stability for nuclear waste storage. *Clay Minerals* 33, 187-196.
- 955 Misra, U., Upchurch, W., 1976. Free energy of formation of beidellite from apparent solubility  
956 measurements. *Clays and Clay Minerals* 24, 327-331.
- 957 Olives, J., Amouric, M., Perbost, R., 2000. Mixed layering of illite-smectite: Results from high-  
958 resolution transmission electron microscopy and lattice-energy calculations. *Clays and Clay*  
959 *Minerals* 48, 282-289.
- 960 Parkhurst, D.L., Appelo, C., 2013. Description of input and examples for PHREEQC version  
961 3: A computer program for speciation, batch-reaction, one-dimensional transport, and inverse  
962 geochemical calculations. US Geological Survey.
- 963 Reesman, A.L., Keller, W.D., 1968. Aqueous solubility of high alumina and clay minerals.  
964 *American Mineralogist* 53, 929-941.
- 965 Tremosa, J., Gailhanou, H., Chiaberge, C., Castilla, R., Gaucher, E.C., Lassin, A., Gout, C.,  
966 Fialips, C., Claret, F., 2020. Effects of smectite dehydration and illitisation on overpressures  
967 in sedimentary basins: A coupled chemical and thermo-hydro-mechanical modelling  
968 approach. *Marine and Petroleum Geology* 111, 166-178.
- 969 Ulbrich, H.H., Waldbaum, D.R., 1976. Structural and other contributions to the third-law  
970 entropies of silicates. *Geochimica et Cosmochimica Acta* 40, 1-24.
- 971 Van Hinsberg, V.J., Vriend, S.P., Schumacher, J.C., 2005a. A new method to calculate end-  
972 member thermodynamic properties of minerals from their constituent polyhedra I: enthalpy,  
973 entropy and molar volume. *Journal of Metamorphic Geology* 23, 165-179.

- 974 Van Hinsberg, V.J., Vriend, S.P., Schumacher, J.C., 2005b. A new method to calculate end-  
975 member thermodynamic properties of minerals from their constituent polyhedra II: heat  
976 capacity, compressibility and thermal expansion. *Journal of Metamorphic Geology* 23, 681-  
977 693.
- 978 Velde, B., 1992. The stability of clays, in: Price, G.D., Ross, N.L. (Eds.), *The Stability of*  
979 *Minerals*. Springer Netherlands, Dordrecht, pp. 329-351.
- 980 Velde, B., Vasseur, G., 1992. Estimation of the diagenetic smectite to illite transformation in  
981 time-temperature space. *American Mineralogist* 77, 967-976.
- 982 Vidal, O., Dubacq, B., 2009. Thermodynamic modelling of clay dehydration, stability and  
983 compositional evolution with temperature, pressure and H<sub>2</sub>O activity. *Geochimica et*  
984 *Cosmochimica Acta* 73, 6544-6564.
- 985 Vieillard, P., 1994a. Prediction of enthalpy of formation based on refined crystal structures of  
986 multisite compounds: Part 1. Theories and examples. *Geochimica et Cosmochimica Acta* 58,  
987 4049-4063.
- 988 Vieillard, P., 1994b. Prediction of enthalpy of formation based on refined crystal structures of  
989 multisite compounds: Part 2. Application to minerals belonging to the system Li<sub>2</sub>O-Na<sub>2</sub>O-K<sub>2</sub>O-  
990 BeO-MgO-CaO-MnO-FeO-Fe<sub>2</sub>O<sub>3</sub>-Al<sub>2</sub>O<sub>3</sub>-SiO<sub>2</sub>-H<sub>2</sub>O. Results and discussion. *Geochimica et*  
991 *Cosmochimica Acta* 58, 4065-4107.
- 992 Vieillard, P., 2000. A new method for the prediction of Gibbs free energies of formation of  
993 hydrated clay minerals based on the electronegativity scale. *Clays and Clay Minerals* 48,  
994 459-473.
- 995 Vieillard, P., 2002. A new method for the prediction of Gibbs free energies of formation of  
996 phyllosilicates (10 Å and 14 Å ) based on the electronegativity scale. *Clays and Clay*  
997 *Minerals* 50, 352-363.
- 998 Vieillard, P., Gailhanou, H., Lassin, A., Blanc, P., Bloch, E., Denoyel, R., Gaboreau, S.,  
999 Fialips, C.I., Made, B., 2019. A predictive model of thermodynamic entities of hydration for  
1000 smectites: application to the formation properties of smectites. *Applied Geochemistry* 110,  
1001 104423.
- 1002 Vieillard, P., Tardy, Y., 1988. Estimation of enthalpies of formation of minerals based on their  
1003 refined crystal structures. *American Journal of Science* 288, 997-1040.
- 1004 Vinograd, V.L., 1995. Substitution of <sup>[4]</sup>Al in layer silicates: Calculation of the Al-Si  
1005 configurational entropy according to <sup>29</sup>Si NMR Spectra. *Physics and Chemistry of Minerals*  
1006 22, 87-98.
- 1007 Wertz, F., Gherardi, F., Blanc, P., Bader, A.-G., Fabbri, A., 2013. Cement CO<sub>2</sub>-alteration  
1008 propagation at the well–caprock–reservoir interface and influence of diffusion. *International*  
1009 *Journal of Greenhouse Gas Control* 12, 9-17.
- 1010 Yamada, H., Yoshioka, K., Tamura, K., Fujii, K., Nakazawa, H., 1999. Compositional gap in  
1011 dioctahedral-trioctahedral smectite system: beidellite-saponite pseudo-binary join. *Clays and*  
1012 *Clay Minerals* 47, 803-810.  
1013  
1014

Annex 1 – I/S mineral compositions and thermodynamic properties calculated for the WS4 Shinzan series

Table A1 - I/S compositions and thermodynamic properties calculated using IStherm, for the WS4 Shinzan series.

Formula	% illite	$\Delta H_f^0$ kJ.mol <sup>-1</sup>	$S^0$ J.mol <sup>-1</sup> .K <sup>-1</sup>	$C_p^0$ J.mol <sup>-1</sup> .K <sup>-1</sup>	$V^0$ cm <sup>3</sup> .mol <sup>-1</sup>
Sample B from Gailhanou (2005) and Gailhanou et al. (2019) <sup>(1)</sup> (K <sub>0.15</sub> Na <sub>0.23</sub> Ca <sub>0.06</sub> )(Mg <sub>0.4</sub> FeII <sub>0.04</sub> Al <sub>1.49</sub> FeIII <sub>0.11</sub> )(Si <sub>3.82</sub> Al <sub>0.18</sub> )O <sub>10</sub> (OH) <sub>2</sub>	15				
Anhydrous minerals					
(K <sub>0.014</sub> Na <sub>0.275</sub> Ca <sub>0.072</sub> )(Mg <sub>0.437</sub> Fe <sub>0.164</sub> Al <sub>1.439</sub> )(Si <sub>3.925</sub> Al <sub>0.075</sub> )O <sub>10</sub> (OH) <sub>2</sub>	0	-5641.05	297.99	314.45	135.97
(K <sub>0.098</sub> Na <sub>0.248</sub> Ca <sub>0.065</sub> )(Mg <sub>0.414</sub> Fe <sub>0.156</sub> Al <sub>1.47</sub> )(Si <sub>3.861</sub> Al <sub>0.139</sub> )O <sub>10</sub> (OH) <sub>2</sub>	10	-5665.14	301.93	315.81	136.37
(K <sub>0.181</sub> Na <sub>0.22</sub> Ca <sub>0.058</sub> )(Mg <sub>0.392</sub> Fe <sub>0.147</sub> Al <sub>1.501</sub> )(Si <sub>3.796</sub> Al <sub>0.204</sub> )O <sub>10</sub> (OH) <sub>2</sub>	20	-5689.33	304.63	317.16	136.77
(K <sub>0.265</sub> Na <sub>0.193</sub> Ca <sub>0.05</sub> )(Mg <sub>0.369</sub> Fe <sub>0.139</sub> Al <sub>1.532</sub> )(Si <sub>3.732</sub> Al <sub>0.268</sub> )O <sub>10</sub> (OH) <sub>2</sub>	30	-5713.46	306.79	318.52	137.17
(K <sub>0.348</sub> Na <sub>0.165</sub> Ca <sub>0.043</sub> )(Mg <sub>0.347</sub> Fe <sub>0.13</sub> Al <sub>1.563</sub> )(Si <sub>3.667</sub> Al <sub>0.333</sub> )O <sub>10</sub> (OH) <sub>2</sub>	40	-5737.41	308.55	319.88	137.57
(K <sub>0.432</sub> Na <sub>0.138</sub> Ca <sub>0.036</sub> )(Mg <sub>0.324</sub> Fe <sub>0.122</sub> Al <sub>1.595</sub> )(Si <sub>3.603</sub> Al <sub>0.397</sub> )O <sub>10</sub> (OH) <sub>2</sub>	50	-5761.05	309.96	321.23	137.97
(K <sub>0.516</sub> Na <sub>0.11</sub> Ca <sub>0.029</sub> )(Mg <sub>0.301</sub> Fe <sub>0.113</sub> Al <sub>1.626</sub> )(Si <sub>3.538</sub> Al <sub>0.462</sub> )O <sub>10</sub> (OH) <sub>2</sub>	60	-5784.27	311.03	322.59	138.37
(K <sub>0.599</sub> Na <sub>0.083</sub> Ca <sub>0.022</sub> )(Mg <sub>0.279</sub> Fe <sub>0.104</sub> Al <sub>1.657</sub> )(Si <sub>3.474</sub> Al <sub>0.526</sub> )O <sub>10</sub> (OH) <sub>2</sub>	70	-5807.01	311.75	323.94	138.77
(K <sub>0.683</sub> Na <sub>0.055</sub> Ca <sub>0.014</sub> )(Mg <sub>0.256</sub> Fe <sub>0.096</sub> Al <sub>1.688</sub> )(Si <sub>3.409</sub> Al <sub>0.591</sub> )O <sub>10</sub> (OH) <sub>2</sub>	80	-5829.19	312.08	325.30	139.17
(K <sub>0.766</sub> Na <sub>0.027</sub> Ca <sub>0.007</sub> )(Mg <sub>0.234</sub> Fe <sub>0.087</sub> Al <sub>1.719</sub> )(Si <sub>3.345</sub> Al <sub>0.655</sub> )O <sub>10</sub> (OH) <sub>2</sub>	90	-5850.76	311.86	326.66	139.56
(K <sub>0.85</sub> )(Mg <sub>0.211</sub> Fe <sub>0.079</sub> Al <sub>1.75</sub> )(Si <sub>3.28</sub> Al <sub>0.72</sub> )O <sub>10</sub> (OH) <sub>2</sub>	100	-5871.70	310.40	328.01	139.96
Hydrated minerals					
(K <sub>0.014</sub> Na <sub>0.275</sub> Ca <sub>0.072</sub> )(Mg <sub>0.437</sub> Fe <sub>0.164</sub> Al <sub>1.439</sub> )(Si <sub>3.925</sub> Al <sub>0.075</sub> )O <sub>10</sub> (OH) <sub>2</sub> ·3.23H <sub>2</sub> O	0	-6583.86	484.94	557.12	194.34
(K <sub>0.098</sub> Na <sub>0.248</sub> Ca <sub>0.065</sub> )(Mg <sub>0.414</sub> Fe <sub>0.156</sub> Al <sub>1.47</sub> )(Si <sub>3.861</sub> Al <sub>0.139</sub> )O <sub>10</sub> (OH) <sub>2</sub> ·2.91H <sub>2</sub> O	10	-6513.67	470.19	534.21	188.90
(K <sub>0.181</sub> Na <sub>0.22</sub> Ca <sub>0.058</sub> )(Mg <sub>0.392</sub> Fe <sub>0.147</sub> Al <sub>1.501</sub> )(Si <sub>3.796</sub> Al <sub>0.204</sub> )O <sub>10</sub> (OH) <sub>2</sub> ·2.58H <sub>2</sub> O	20	-6443.58	454.20	511.30	183.46
(K <sub>0.265</sub> Na <sub>0.193</sub> Ca <sub>0.05</sub> )(Mg <sub>0.369</sub> Fe <sub>0.139</sub> Al <sub>1.532</sub> )(Si <sub>3.732</sub> Al <sub>0.268</sub> )O <sub>10</sub> (OH) <sub>2</sub> ·2.26H <sub>2</sub> O	30	-6373.43	437.66	488.39	178.03
(K <sub>0.348</sub> Na <sub>0.165</sub> Ca <sub>0.043</sub> )(Mg <sub>0.347</sub> Fe <sub>0.13</sub> Al <sub>1.563</sub> )(Si <sub>3.667</sub> Al <sub>0.333</sub> )O <sub>10</sub> (OH) <sub>2</sub> ·1.94H <sub>2</sub> O	40	-6303.09	420.72	465.48	172.59
(K <sub>0.432</sub> Na <sub>0.138</sub> Ca <sub>0.036</sub> )(Mg <sub>0.324</sub> Fe <sub>0.122</sub> Al <sub>1.595</sub> )(Si <sub>3.603</sub> Al <sub>0.397</sub> )O <sub>10</sub> (OH) <sub>2</sub> ·1.62H <sub>2</sub> O	50	-6232.45	403.44	442.57	167.15
(K <sub>0.516</sub> Na <sub>0.11</sub> Ca <sub>0.029</sub> )(Mg <sub>0.301</sub> Fe <sub>0.113</sub> Al <sub>1.626</sub> )(Si <sub>3.538</sub> Al <sub>0.462</sub> )O <sub>10</sub> (OH) <sub>2</sub> ·1.29H <sub>2</sub> O	60	-6161.40	385.81	419.66	161.71
(K <sub>0.599</sub> Na <sub>0.083</sub> Ca <sub>0.022</sub> )(Mg <sub>0.279</sub> Fe <sub>0.104</sub> Al <sub>1.657</sub> )(Si <sub>3.474</sub> Al <sub>0.526</sub> )O <sub>10</sub> (OH) <sub>2</sub> ·0.97H <sub>2</sub> O	70	-6089.85	367.84	396.75	156.28
(K <sub>0.683</sub> Na <sub>0.055</sub> Ca <sub>0.014</sub> )(Mg <sub>0.256</sub> Fe <sub>0.096</sub> Al <sub>1.688</sub> )(Si <sub>3.409</sub> Al <sub>0.591</sub> )O <sub>10</sub> (OH) <sub>2</sub> ·0.65H <sub>2</sub> O	80	-6017.75	349.47	373.83	150.84
(K <sub>0.766</sub> Na <sub>0.027</sub> Ca <sub>0.007</sub> )(Mg <sub>0.234</sub> Fe <sub>0.087</sub> Al <sub>1.719</sub> )(Si <sub>3.345</sub> Al <sub>0.655</sub> )O <sub>10</sub> (OH) <sub>2</sub> ·0.32H <sub>2</sub> O	90	-5945.04	330.56	350.92	145.40

(1) Ti (0.006 cations per O<sub>10</sub>(OH)<sub>2</sub>, in original B sample) is replaced by Al, for sake of simplicity.

# Computing tool

Electronegativity model  
 $\Delta H_f^0$

Configuration entropy  
 $S_{\text{conf}}$

Polyhedral model  
 $S_{\text{cal}}^0, C_p^0, V^0$

$\Delta \Xi_f^0$   
(anhydrous)

+

$\Delta \Xi_{\text{hyd}}^0$   
(hydration)

+

$\Delta \Xi_f^0$   
(H<sub>2</sub>O)

Hydration model  
 $\Delta H_{\text{hyd}}^0, \Delta S_{\text{hyd}}^0, n\text{H}_2\text{O}$

Bulk water properties

=

$\Delta \Xi_f^0$  (Hydrated clay mineral)

